Regulatory T cells are expanded by Teriparatide treatment in humans and mediate intermittent PTH-induced bone anabolism in mice

Regulatory T cells are expanded by Teriparatide treatment in humans and mediate intermittent PTH-induced bone anabolism in mice

Mingcan Yu, Patrizia D'Amelio, Abdul Malik Tyagi, Chiara Vaccaro, Jau-Yi Li, Emory Hsu, Ilaria Buondonno, Francesca Sassi, Jonathan Adams, M Neale Weitzmann, Richard DiPaolo, Roberto Pacifici

EMBO Rep. 2017 Nov 20. pii: e201744421. doi: 10.15252/embr.201744421. [Epub ahead of print]

REGULATORY T CELLS ARE EXPANDED BY TERIPARATIDE TREATMENT IN HUMANS AND MEDIATE INTERMITTENT PTH-INDUCED BONE ANABOLISM IN MICE

Mingcan Yu[1], Patrizia D'Amelio[2], Abdul Malik Tyagi[1], Chiara Vaccaro[1], Jau-Yi Li[1], Emory Hsu[1], Ilaria Buondonno[2], Francesca Sassi[2], Jonathan Adams[1], M. Neale Weitzmann[1,3], Richard DiPaolo[4], and Roberto Pacifici[1,5]

[1]Division of Endocrinology, Metabolism and Lipids, Department of Medicine, Emory University, Atlanta, GA, [2]Gerontology Section, Department of Medical Sciences, University of Torino, Corso Bramante 88/90, 10126 Torino, Italy, [3]Atlanta Department of Veterans Affairs Medical Center, Decatur, GA 30033, [4]Department of Molecular Microbiology & Immunology, Saint Louis University School of Medicine, St. Louis Missouri 63104, [5]Immunology and Molecular Pathogenesis Program, Emory University, Atlanta, GA.

The authors have declared that no conflict of interest exists
Classification: Biological Sciences

Key Words: PTH, T cells, Regulatory T cells, Wnt10b, NFAT, SMAD, bone

Running title: Regulatory T cells mediate PTH induced anabolism

Nonstandard abbreviations used: Bone marrow (BM), Intermittent PTH (iPTH), Parathyroid hormone (PTH), Regulatory T cells (Tregs) PTH/PTHrP receptor (PPR), Stromal cells (SCs).

Address correspondence to:

Roberto Pacifici, M.D.
Division of Endocrinology, Metabolism and Lipids
Emory University School of Medicine
101 Woodruff Circle, Room 1309
Atlanta, GA 30322
Telephone: 404-712-8420
Fax: 404-727-1300
E-mail: roberto.pacifici@emory.edu

ABSTRACT

Teriparatide is a bone anabolic treatment for osteoporosis, modeled in animals by intermittent PTH (iPTH) administration. iPTH-induced bone anabolism involves CD8+ T cell production of the osteogenic Wnt ligand Wnt10b, induced via yet unknown mechanisms. Here we show that Teriparatide and iPTH cause a ~2-3-fold increase in the number of regulatory T cells (Tregs) in humans and mice. Attesting in vivo relevance, blockade of the Treg increase in mice prevents iPTH-induced CD8+ T cell Wnt10b production and bone anabolism. Mechanistically, Treg action on CD8+ T cells promotes binding of NFAT1/2 and SMAD3 complexes to a NFAT/SMAD-activated Wnt10b promoter region that stimualtes Wnt10b gene expression in CD8+ T cells. Therefore, increasing the number of Tregs is a pivotal mechanism by which iPTH exerts its bone anabolic activity. Increasing Tregs pharmacologically may represent a novel bone anabolic therapy, while iPTH-induced Treg increase may find applications in inflammatory conditions and transplant medicine.

INTRODUCTION

Primary hyperparathyroidism is a common cause of bone loss and fractures due to the continuous production of high levels of PTH by the parathyroid glands (Grey, Stapleton et al., 1996, Potts, 1998). By contrast, when PTH is injected daily, a regimen known as intermittent PTH (iPTH) treatment, the hormone increases bone volume and strength due to a stimulation of bone formation tempered by a more moderate increase in resorption (Jilka, 2007, Uzawa, Hori et al., 1995). As a result, intermittent treatment with the 1- 34 fragment of PTH is an FDA-approved treatment modality for postmenopausal osteoporosis (Zaidi, 2007).

PTH acts by binding to the PTH/PTHrP receptor PPR, which is expressed in all osteoblastic cells, including stromal cells (SCs), osteoblasts, and osteocytes (Calvi, Sims et al., 2001, Lanske, Amling et al., 1999, Powell, Barry et al., 2011, Rhee, Allen et al., 2011, Saini, Marengi et al., 2013). Moreover, PPR is expressed in conventional CD4+ and CD8+ T cells (Terauchi, Li et al., 2009) and macrophages (Cho, Soki et al., 2014). iPTH stimulates bone formation by increasing osteoblast formation and lifespan. Activation of Wnt signaling in osteocytes and osteoblasts is one of the proposed mechanisms by which iPTH stimulates bone formation (Jilka, 2007, Kramer, Loots et al., 2010, Qin, Raggatt et al., 2004). Wnt signaling activation is achieved through multiple mechanisms including Wnt ligand-independent activation of Wnt coreceptors (Wan, Yang et al., 2008), blunted osteocytic production of the Wnt inhibitor sclerostin (Bellido, Ali et al., 2005, Keller & Kneissel, 2005, Silvestrini, Ballanti et al., 2007) and decreased production by osteoblasts of the Wnt inhibitor Dkk1 (Guo, Liu et al., 2010).

While osteocytes and their production of sclerostin are critical for the activity of iPTH, part of this hormone activity is sclerostin independent (Li, Walker et al., 2014) and mediated by T cells (Pacifici, 2013), a cell lineage that potentiates the anabolic activity of iPTH in trabecular bone (Bedi, Li et al., 2012, Li et al., 2014, Terauchi et al., 2009). Accordingly, iPTH fails to stimulate bone formation and increase bone mass in T cell null mice (Terauchi et al., 2009). By contrast,

the effects of iPTH in cortical bone are completely T cell independent (Bedi et al., 2012, Li et al., 2014, Terauchi et al., 2009), likely due to the fact that T cells have no contacts with periosteal surfaces and have limited capacity to communicate with osteocytes. Among the T cells required for iPTH to exert its full anabolic activity are bone marrow (BM) CD8+ T cells (Terauchi et al., 2009). CD8+ T cells express higher levels of the receptor PPR than CD4+ T cells (Bedi et al., 2012, Li et al., 2014, Terauchi et al., 2009). Moreover, BM CD8+ T cells, but not CD4+ T cells, respond to iPTH by releasing Wnt10b (Bedi et al., 2012, Li et al., 2014, Terauchi et al., 2009), an osteogenic Wnt ligand that activates Wnt signaling in osteoblastic cells (Bennett, Ouyang et al., 2007). Accordingly, silencing of Wnt10b production by CD8+ T cells blocks the capacity of iPTH to activate Wnt signaling in osteoblasts, stimulate bone formation and increase trabecular bone volume (Bedi et al., 2012, Li et al., 2014, Terauchi et al., 2009). The relevance of Wnt10b has been confirmed in human studies demonstrating that treatment with Teriparatide, a form of iPTH treatment, increases the production of Wnt10b by peripheral blood T cells (D'Amelio, Sassi et al., 2015). However, the mechanism by which iPTH regulates Wnt10b production remains to be determined.

Regulatory T cells (Tregs) are a suppressive population of predominantly CD4+ T cells that play a critical role in maintaining immune tolerance and immune homeostasis. Tregs are comprised of thymus derived Tregs (tTregs, also known as nTregs) and peripherally derived Tregs (pTregs, also known as iTregs) (Abbas, Benoist et al., 2013). Tregs are defined by the expression of the transcription factor Foxp3 and the ability to block inflammatory diseases and maintain immune homeostasis and tolerance (Shevach, 2009). Accordingly, defects in Treg numbers and/or activity have been implicated in several chronic inflammatory diseases. Moreover, Tregs have furthermore been found blunt bone resorption (Kim, Lee et al., 2007, Yuan, Li et al., 2010), prevent ovariectomy induced bone loss (Zaiss, Sarter et al., 2010), and regulate osteoclast formation (Kelchtermans, Geboes et al., 2009, Kim et al., 2007, Zaiss, Axmann et al., 2007).

In vitro, conventional CD4+ T cells differentiate into Tregs by TCR stimulation under the influence of TGFβ and IL-2 (Chen, Jin et al., 2003, Liu, Zhang et al., 2008, Ohkura, Kitagawa et al., 2013) . Recently, IGF-1 has been recognized as an additional inducer of Tregs (Anguela, Tafuro et al., 2013, Johannesson, Sattler et al., 2014). Since iPTH increases TGFβ and IGF-1 production in bone (Cho, Pirih et al., 2013, McCarthy, Centrella et al., 1989, Pfeilschifter, Laukhuf et al., 1995), it is likely that iPTH may induce and/or expand BM Tregs.

This study was designed to investigate the effects of iPTH on Treg formation and activity in humans and mice, and to determine whether Tregs play a role in the bone anabolic activity of iPTH in mice. We report that treatment with iPTH increases the number of Tregs in humans and mice. In rodents, an increase in the number of Tregs is required for iPTH to exert its bone anabolic activity. We also show that in mice the increase in Tregs induced by iPTH activates NFAT1/2 and SMAD2/3 signaling in CD8+ T cells and blunts CD28 signaling in CD8+ T cells. These effects allow iPTH to upregulate the binding of NFAT/SMAD complexes to a site in the Wnt10b promoter critical for Wnt10b gene expression in CD8+ T cells. Therefore, Tregs play a pivotal role in the production of Wnt10b and the resulting bone anabolic activity of iPTH.

RESULTS

Teriparatide treatment increases the number of Tregs in human peripheral blood

The PTH fragment Teriparatide is the only approved bone anabolic treatment for osteoporosis but its intricate mechanism of action remains largely unknown. Among the pleiotropic effects of PTH, is the capacity to increase the production of TGFβ1 and IGF-1 by human osteoblasts (Esen, Lee et al., 2015, Oursler, Cortese et al., 1991, Wu & Kumar, 2000), factors which induce Treg differentiation. To investigate whether Teriparatide regulates the number of Tregs in humans, 40 Italian women afflicted by postmenopausal osteoporosis of similar age and years since menopause were enrolled in a 6 month long prospective clinical trial. Twenty of the 40 women were treated with calcium and vitamin D (control treatment), while the remaining 20 women were treated with calcium, vitamin D, and human PTH 1-34 (Teriparatide), a treatment modality referred to hereafter as Teriparatide treatment. The baseline demographic characteristics of the study population and the serum levels of calcium, PTH and 25-hydroxy Vitamin D are shown in **Table 1**. Peripheral blood mononuclear cells (PBMC) were obtained at baseline, 3 and 6 months of treatment. Analysis by flow cytometry revealed that Teriparatide treatment increased the absolute and relative number of Tregs (CD4+CD25+Foxp3+ cells) in human PBMC at 3 and 6 months of treatment, compared to baseline **(figure 1A,B**). By contrast, treatment with calcium and Vitamin D did not alter the number of Tregs during the 6 months of the study. As a result, both at 3 and 6 months the absolute and relative number of Tregs in PBMC was higher in women treated with Teriparatide than in those in the calcium and vitamin D control group.

TGFβ1 not only is a critical inducer of Treg differentiation, but is also an important product of Tregs that contributes to suppress effector T cells in vivo (Chaudhry & Rudensky, 2013,

Shevach, 2009). Production of TGFβ1 by Tregs is therefore an indicator of Treg function. To determine if Teriparatide regulates the function of Tregs, we measured the level of TGFβ1 mRNA in sorted peripheral blood CD4+CD25+ T cells from the last 18 women enrolled in the trial. We selected this cell population because most CD4+CD25+ T cells are Foxp3+ Tregs, while measurements of TGFβ1 mRNA in Tregs sorted by Foxp3 staining is not feasible due to the loss of cell viability caused by intracellular staining. We found that the level of TGFβ1 mRNA in this Treg enriched population was higher in the Teriparatide treated group than in the control group **(figure 1C**). Post-hoc analysis showed that TGFβ1 mRNA levels were higher at 3 months than at baseline in the Teriparatide treated group. Moreover, at 6 months TGFβ1 mRNA levels were higher in the Teriparatide treated group than in the control group. Together, these findings demonstrate that Teriparatide treatment expands the number and the activity of circulating human Tregs.

To determine whether Teriparatide targets Tregs directly or indirectly, human peripheral blood CD4+CD25+ T cells were stimulated in vitro with CD3/CD28 Ab, IL-2 and TGFβ at 2.5 ng/ml for 6 days. Vehicle or Teriparatide (50 ng/ml) were added every 2 days for 1 or 24 hours. Analysis by flow cytometry revealed that Teriparatide did not increase the relative number of Tregs (CD4+CD25+Foxp3+ cells) in cultures of peripheral blood CD4+CD25+ T cells **(figure 1D**), suggesting that Teriparatide regulates the number of Tregs via indirect mechanisms. We also found that in vitro stimulation with Teriparatide does not increase the expression of TGFβ mRNA in in sorted peripheral blood CD4+CD25+ T cells **(figure 1E**), confirming that Teriparatide does not directly targets Tregs.

IPTH treatment in mice expands the pool of murine BM Tregs by increasing Treg differentiation

As in human cells, in vitro PTH stimulation increases of production of TGFβ1 and IGF-1 by murine osteoblasts (Cho et al., 2013, McCarthy et al., 1989, Pfeilschifter et al., 1995). However, the effects of iPTH treatment on the production of these factors is largely unknown. To investigate this matter, 6 weeks old mice were treated with vehicle or iPTH for 2 weeks. BM was then harvested and cultured for 24 hours. ELISA assays revealed that iPTH significantly increases the levels of TGFβ1 and IGF-1 in the whole BM culture media (**Supplemental figure 1A,B**), suggesting that iPTH may regulate Treg differentiation.

To investigate the effect of iPTH treatment on the number of BM Tregs, 6-week-old mice were treated with vehicle or iPTH for 1, 2 or 4 weeks. BM was then harvested and stained for TCRβ, CD4 and Foxp3. iPTH treatment increased the relative and absolute number of BM Tregs (TCRβ+CD4+Foxp3+ cells) during the entire study period **(figure 2A,B)**. The increase in absolute number of BM Tregs was already significant at 1 week of iPTH treatment, peaked at 2 weeks**,** and remained significantly increased at 4 weeks of treatment.

iPTH could expand the pool of BM Tregs via multiple mechanisms including increasing the differentiation of conventional CD4+ T cells into Tregs or the proliferation of Tregs within the BM. To gain mechanistic insights, we determined the effects of iPTH on Treg differentiation, which is defined as the induction of Foxp3 expression in CD4+Foxp3- T cells (Shevach, 2009). For this purpose, we made use of B6.Foxp3.eGFP reporter mice, a strain in which eGFP expression is co-expressed with Foxp3 and restricted to CD4+ T cells. Conventional CD4+ T cells (CD4+eGFP-) were FACS sorted from the spleens of B6.Foxp3.eGFP reporter mice and transferred into TCRβ-/-mice, a strain lacking αβ T cells. After 2 weeks, a length of time sufficient for the engraftment and expansion of donor T cells, recipient mice were treated with

vehicle or iPTH for 1-4 weeks. We then determined the number of CD4+eGFP+ cells in the BM by flow cytometry. Treatment with iPTH increased the relative and the absolute number of CD4+eGFP+ cell in the BM at 1 week, 2 weeks, and 4 weeks of treatment (**figure 2 C,D**), demonstrating that iPTH increases the differentiation of BM Tregs. Additional studies that used BrdU incorporation to measure proliferation, revealed that iPTH treatment for 1, 2 or 4 weeks does not increase BM Treg proliferation (**Supplemental figure 2A**). Analysis of Treg differentiation in other organs revealed that iPTH treatment did not increase the differentiation of Tregs in the spleen (**Supplemental figure 2B,C**), thymus (**Supplemental figure 2D,E**), and intestinal lamina propria (**Supplemental figure 2F**). In an additional set of experiments, Tregs (CD4+eGFP+ cells) were FACS sorted from the spleens of B6.Foxp3.eGFP reporter mice and transferred into TCRβ-/-mice. Recipient mice were treated with vehicle or iPTH for 2 weeks, starting the day of the Treg transfer. This design was selected to minimize the confounding effect of the partial loss of Foxp3 expression by CD4+eGFP+ cells, which may occur after Treg transfer into lymphopenic host mice (Duarte, Zelenay et al., 2009). These studies revealed that iPTH does not affect the relative and the absolute number of CD4+eGFP+ cells residing in the spleen and BM (**Supplemental figure G-J**). These findings, together with a lack of an effect of iPTH on Treg proliferation, indicate that iPTH does not alter the homing of Tregs to the spleen and the BM.

In addition to increasing the BM levels of TGFβ and IGF-1 (Cho et al., 2013, McCarthy et al., 1989, Pfeilschifter et al., 1995), iPTH enhances the sensitivity of conventional CD4+ cells to TGFβ. This was disclosed by experiments in which unstimulated splenic CD4+CD25- cells purified from iPTH treated mice were found to express lower levels of the negative regulator of TGFβ signaling SMAD7 as compared to CD4+CD25- cells from vehicle treated mice **(supplemental figure 3A)**. To ascertain the functional relevance of this finding, splenic CD4+CD25- cells from vehicle or iPTH treated mice were stimulated in vitro with CD3/CD28 Ab,

IL-2 and TGFβ at 2.5 ng/ml for 72 hours to induce their differentiation into Tregs (Karlsson, Robinson-Jackson et al., 2011). Measurements of phosphorylated SMAD2 and SMAD3 (pSMAD2 and pSMAD3) at the end of the culture period revealed higher concentrations of pSMAD2 and pSMAD3 **(supplemental figure 3B)** in cells from iPTH treated mice as compared to those from control mice, suggesting that conventional CD4+ T cells from iPTH treated mice have a higher sensitivity to TGFβ. To confirm this hypothesis, splenic CD4+CD25- cells were purified from vehicle or iPTH treated mice and then cultured in vitro for 72 hours with anti CD3/CD28 Ab, IL-2 and increasing doses of TGFβ (0.1-5 ng/ml). At each dose of TGFβ, cultures of CD4+CD25- T cells from iPTH treated mice yielded a greater percentage of Foxp3+ Tregs than those from vehicle treated mice **(supplemental figure 3C).** Together, these findings indicate that CD4+ T cells from iPTH treated mice possess a greater sensitivity to TGFβ, which results in enhanced differentiation of CD4+ T cells into Tregs.

An increase in the number of Tregs is required for iPTH to induce bone anabolism in mice

A direct means to investigate the contribution of Tregs to the anabolic activity of iPTH is to assess the effects of iPTH in a model in which the increase in the frequency of Tregs is prevented. The surface marker CD25 is expressed at high levels by most CD4+ Foxp3+ Tregs (Roncador, Brown et al., 2005). Accordingly, treatment with anti-CD25 Abs capable of deleting $CD25^{hi}$ is used to partially deplete Tregs in vivo (Setiady, Coccia et al., 2010, Tan, Reddy et al., 2013). We thus treated 6-week-old mice with vehicle or iPTH (days 1-28) plus 4 injections (days -2,0,5, and 7) of isotype control Ab or the anti-CD25 Ab PC61 (Setiady et al., 2010, Tan et al., 2013). We found $CD25^{hi}$ to be expressed by CD4+ T cells and by a negligible fraction of CD8+ T cells **(supplemental figure 4A).** Anti-CD25 Ab decreased the frequency of $CD25^{hi}$

CD4+ T cells but not that of $CD25^{lo}$ CD4+ T cells. As previously reported (Betts, Ho et al., 2011), we also found that treatment with anti-CD25 Ab decreased the number of $CD25^{hi}$Foxp3+CD4+ T cells, but not the number of $CD25^{lo}$FoxP3-CD4+ T cells **(supplemental figure 4B**). In addition, treatment with anti-CD25 Ab did not decrease the percentage of BM of conventional CD4+ T cells (TCRβ+CD4+CD25+Foxp3- cells) and that of CD8+ T cells (TCRβ+CD8+CD25+ cells) (**supplemental figure 4C**). Together, these findings demonstrate that anti-CD25 Ab specifically deplete Tregs.

At sacrifice control mice treated with anti-CD25 Ab had ~37 % fewer Tregs than mice treated with irrelevant (Irr.) Ab **(figure 3A,B)**. Moreover, treatment with anti-CD25 Ab prevented the increase in BM Tregs induced by iPTH**.** The partial depletion of Tregs induced by anti-CD25 Ab did not increase the production of inflammatory and lineage specific cytokines in the BM. In fact, in both the vehicle and iPTH treated groups, BM cells from mice treated with anti-CD25 Ab expressed similar levels of TNF, IL-17A, IL-6, IL-4 and IL-13 mRNAs to those from mice treated with Irr. Ab **(Supplemental figure 5)**. Moreover, iPTH lowered the mRNA levels of IFNγ, in both the Irr. Ab and the anti-CD25 Ab groups but did not affect the other cytokines. Since inflammatory cytokines blunt bone formation (Bertolini, Nedwin et al., 1986), these findings indicate treatment with anti CD25 Ab does not alter the bone anabolic activity of iPTH by inducing inflammation. Blockade of the increase in the number of Tregs by anti-CD25 Ab was associated with the loss of the capacity of iPTH to stimulate Wnt10b mRNA expression in T cells **(figure 3C)**, a factor responsible for the bone anabolic activity of iPTH**.** Analysis by in vitro μCT of femurs harvested at sacrifice revealed that iPTH induced a significant increase in trabecular bone volume (BV/TV) in mice treated with Irr. Ab **(figure 3D,E)**, but not in those treated with anti-CD25 Ab. Trabecular thickness (Tb.Th), trabecular number (Tb.N), and trabecular space (Tb.Sp), which are indices of trabecular structure, were altered by iPTH in mice treated with Irr. Ab, but not in those treated with anti-CD25 Ab (**Supplemental figure 6A-**

C). By contrast, iPTH increase cortical volume (Ct.Vo) **(figure 3D,F)** and cortical thickness (Ct.Th) (**Supplemental figure 6D**) in both groups of mice, confirming that T cells are not implicated in the mechanism by which iPTH increases cortical volume. Together, these findings demonstrate that the anabolic effects of iPTH in trabecular bone are dependent on increased numbers of Tregs.

Analysis of femoral cancellous bone by histomorphometry revealed that iPTH increased the dynamic indices of bone formation mineral apposition rate (MAR) and bone formation rate (BFR/BS) in Treg replete mice but not in those treated with anti-CD25 Ab (**figure 3G-I**). Moreover, iPTH increased two static indices of bone formation, the number of osteoblasts per bone surface (N.Ob/BS) (**figure 3J**) and the percentage of surfaces covered by osteoblasts (Ob.S/BS) (**figure 3K**) in Treg replete mice but not in those treated with anti-CD25 Ab. The finding that treatment with anti-CD25 Ab did not decrease bone formation in vehicle treated mice provide evidence that partial Treg depletion does not cause a nonspecific inhibitory effect of on bone formation. Two indices of bone resorption, the number of OCs per bone surface (N.Oc/BS) and the percentage of surfaces covered by OCs (Oc.S/BS) were not affected by iPTH (**figure 3L-N**) in both control and Treg depleted groups. However, N.Oc/BS was higher in mice treated with iPTH and CD25 Ab, as compared to those treated with iPTH and Irr. Ab, suggesting that Treg depletion may stimulate bone resorption.

Measurements of serum levels of osteocalcin, a marker for bone formation revealed that iPTH increased bone formation in mice treated with Irr. Ab but not in those treated with anti-CD25 Ab (**figure 3O**). Serum CTX, a marker for bone resorption, also increased significantly in response to iPTH in mice treated with Irr. Ab but not in those injected with anti-CD25 Ab (**figure 3P)**. Moreover, mice treated with anti-CD25 Ab had higher CTX levels than those treated with Irr. Ab, confirming that Treg depletion is associated with an increase in bone resorption. The differences between the CTX data and histomorphometric indices of bone resorption are

explained by the fact that CTX reflects cortical and trabecular bone resorption, while the histomorphometric analysis was limited to the trabecular compartment.

To determine the role of Tregs in mediating the effects of iPTH on osteoblastogenesis, BM was harvested at sacrifice and cultured for 1 week to allow SCs to proliferate. SCs were then purified and counted. This analysis revealed that iPTH treatment increases the number of SCs in samples from mice treated with Irr. Ab while it had no effects in those treated with anti-CD25 Ab (**Supplemental figure 7A**). To investigate the mechanism involved, BM was cultured for 1 week, and SCs purified and used to determine their rate of proliferation and apoptosis. These experiments revealed that iPTH increases significantly the proliferation of SCs from mice treated with Irr. Ab, while it had no effect on the proliferation of SCs from mice treated with anti-CD25 Ab (**Supplemental figure 7B**). iPTH decreased the rate of SC apoptosis in mice treated with Irr. Ab, while it had no effect on SC apoptosis in mice treated with anti-CD25 Ab (**Supplemental figure 7C**). Analysis of the expression levels of osteoblastic genes in SCs revealed that iPTH treatment increased the expression of type 1 collagen, Runx2, Osterix, Bone Sialoprotein, and Osteocalcin mRNAs in SCs from mice treated with Irr. Ab, while it had no effect on SCs from mice treated with anti-CD25 Ab **(Supplemental figure 7D)**. These findings demonstrate that iPTH regulates osteoblast proliferation, differentiation and life span through a Treg dependent mechanism.

To further investigate the relevance of Tregs for the anabolic activity of iPTH, experiments were conducted utilizing DEREG mice (Lahl, Loddenkemper et al., 2007), a strain that expresses a fusion protein of the human diphtheria toxin (DT) receptor (hDTR) and eGFP under control of the Foxp3 promoter. Foxp3+ Tregs can be selectively depleted upon DT administration to DEREG mice, since WT mice do not express the hDTR receptor and are thus insensitive to DT. DT is known not to cause toxic effects in mice (Klingenberg, Gerdes et al., 2013). While Treg ablation in DEREG mice causes scurfy-like symptoms in newborn animals, older mice do not develop autoimmune diseases (Klingenberg et al., 2013, Lahl et al., 2007) as

DT treatment of older DEREG mice causes a partial Treg depletion (Lahl & Sparwasser, 2011) and the residual Treg population is sufficient to prevent disease in adult mice (Lahl & Sparwasser, 2011). We treated 6-week-old mice with DT (1 μg/mouse, i.p. 2 times per week for 4 weeks), a treatment modality titrated to block the increase in Tregs induced by iPTH. Mice were also treated with vehicle or iPTH for 4 weeks starting after the first two DT injections. Controls included DEREG mice not treated with DT and WT littermate (LM) mice treated with DT. Analysis of BM samples harvested at sacrifice revealed that iPTH had expanded Tregs in control mice but not in DEREG +DT mice **(figure. 4A,B)**. As expected, analysis of vehicle treated groups showed that DEREG + DT mice had a lower absolute and relative numbers of Tregs as compared to control groups. Analysis of BM T cells harvested at sacrifice revealed that iPTH did not increase Wnt10b mRNA expression in DEREG + DT mice, while it caused significant increases in Wnt10b mRNA levels in the two control groups **(figure 4C).** Analysis by μCT of femurs harvested at sacrifice revealed that iPTH induced a significant increase in BV/TV in the two control groups but not in DT treated DEREG mice **(figure 4D,E)**. Analysis of distal femurs also revealed that Tb.Th, Tb.N, and Tb.Sp were differentially altered by IPTH in Treg replete and Treg depleted mice (**Supplemental figure 6E-G**). By contrast, iPTH increased Ct.Vo **(figure 4D,F)** and cortical thickness (Ct.Th) (**Supplemental figure 6H**) in all groups of mice. Together, these findings confirmed that the anabolic effects of iPTH in trabecular bone are dependent on increased numbers of Tregs.

Analysis of femoral cancellous bone by histomorphometry revealed that iPTH increased the dynamic indices of bone formation MAR and BFR/BS in the two control groups but not in DT treated DEREG mice (**figure 4G-I**). N.Ob/BS and Ob.S/BS, which are static indices of bone formation, were also increased by iPTH in DEREG mice and littermate controls but not in DEREG + DT mice (**figure 4J,K**). Two indices of bone resorption, N.Oc/BS and Oc.S/BS were similar in all groups of mice (**figure 4L-N**). Analysis of biochemical markers of bone turnover

revealed that iPTH increased serum level of osteocalcin and CTX in control mice but not on Treg depleted mice (**figure 4O,P**), confirming that the increase in the number of BM Treg is required for iPTH to increase bone turnover. In vehicle treated mice, serum CTX was higher in Treg depleted mice that in Treg replete controls, confirming that Treg depletion leads to a stimulation of bone resorption.

Tregs increase the production of Wnt10b induced by iPTH in mice by blunting CD28 signaling and inducing NFAT and SMAD signaling in CD8+ T cells.

Previous reports have demonstrated that CD8+ T cell produced Wnt10b is critical for the anabolic activity of iPTH in the trabecular compartment of the skeleton (Bedi et al., 2012, Li et al., 2014, Terauchi et al., 2009). The current investigation has revealed that stimulation of CD8+ T cell production of Wnt10b by iPTH is mediated by Tregs. An important issue that remains to be addressed is whether Tregs per se contribute to the increase in the BM levels of Wnt10b induced by iPTH. Studies conducted in sorted populations of BM T cells from B6.Foxp3.eGFP reporter mice revealed that iPTH does not increase the expression of Wnt10b mRNA by conventional CD4+ T cells (TCRβ+CD4+eGFP- cells) and Tregs (TCRβ+CD4+ eGFP + cells) **(figure 5A**). These findings confirm earlier reports from our laboratory (Bedi et al., 2012, Li et al., 2014, Terauchi et al., 2009) and argue against a direct contributory role of Tregs to the pool of BM Wnt10b of iPTH treated mice.

Another pivotal issue is the mechanism by which Tregs regulate the capacity of iPTH to increase Wnt10b production by CD8+ T cells. The NFAT family of transcription factors includes 5 members, NFAT1 to 5, of which NFAT1 (NFATc2) and NFAT2 (NFATc1) play a central role in peripheral CD4+ and CD8+ T cell activation, tolerance, anergy and exhaustion (Fehr, Lucas et al., 2010, Heissmeyer, Macian et al., 2004, Macian, Garcia-Cozar et al., 2002). Activation of calcineurin upon TCR signaling leads to dephosphorylation of NFATs, which then translocate to

the nucleus where they activate transcription by interacting with AP-1 or other nuclear proteins including SMADs (Macian, 2005). The Wnt10b promoter possesses 3 DNA monomeric core binding motifs for NFATs, located in close proximity to binding sites for the TGFβ signaling proteins SMADs. This arrangement suggest that iPTH-induced Wnt10b transcription might be regulated by the binding of NFAT/SMAD dimers to the Wnt10b promoter. This hypothesis is further supported by reports that PTH and PTHrP activate NFAT signaling in osteoblasts (Huang, Chikazu et al., 2010, Park, Baek et al., 2015), by the fact that PTH increases the production of TGFβ by osteoblasts (Pfeilschifter et al., 1995), and by data presented herein indicating that iPTH increases the BM levels of TGFβ1 protein (**Supplemental figure 1**).

To investigate the relevance of SMADs and NFATs for Wnt10b gene expression, we first measured Wnt10b mRNA levels in purified splenic CD8+ T cells after in vitro stimulation with the SMAD inducer TGFβ and the NFAT activator ionomycin. We found that stimulation with both TGFβ and ionomycin markedly increased Wnt10b production while TGFβ or ionomycin alone had a significant, yet less potent, effect **(figure 5B**), indicating a potential role of SMAD and NFAT signaling in Wnt10b gene expression.

To determine if NFATs and SMADs bind to the Wnt10b promoter, ChIP assays were conducted in BM CD8+ T cells from vehicle and iPTH treated mice. We found that CD8+ T cells from iPTH treated mice had higher binding of NFAT1, NFAT2, and SMAD3 (but not SMAD2) to the Wnt10b promoter as compared to CD8+ T cells from vehicle treated mice **(figure 5C**).

Blockade of the increase in the number of Tregs by in vivo treatment with anti-CD25 Ab prevented iPTH from increasing the binding of NFAT1, NFAT2, and SMAD3 to the Wnt10b promoter, thus demonstrating that Tregs are required for iPTH to increase the binding of these transcription factors to the Wnt10b promoter.

To investigate the functional relevance of NFAT/SMAD binding to the Wnt10b promoter we cloned a 2,000 bp upstream region of the mouse Wnt10b gene containing the three putative

NFAT/SMAD binding sites into a luciferase reporter plasmid. The Wnt10b-luc reporter plasmid (or empty vector) together with TK-pRL transfection control vector were transfected into primary murine CD8+ T cells or EL4 cells. After transfection, cells were rested for 24 hours and then stimulated with ionomycin and TGFβ for 24 hours to activate Wnt10b transcription. Cell lysates were then assessed by dual luciferase assay kit, as an index of promoter activity. We found that stimulation with ionomycin and TGFβ increased Wnt10b promoter activity **(figure 5D**). Deletion of the 2 most distal NFAT/SMAD binding sites did not alter the activity of the reporter. By contrast, deletion of all 3 NFAT/SMAD binding sites abolished the activity of the reporter, suggesting that the NFAT/SMAD binding site critical for Wnt10b transcription is located between -705 bp and -272 bp in the Wnt10b promoter. Site directed mutagenesis experiments confirmed **(figure 5E**) that the critical binding site is located between -705 bp and -272 bp in the Wnt10b promoter. Mutation of both the SMAD and the NFAT sites lowered the activity of the reporter in in primary murine CD8+ T cells and EL4 cells to baseline levels. Mutation of the NFAT binding site alone also decreased the activity of the reporter to baseline levels, while mutation of the SMAD site alone resulted in a marked decrease, but not a complete inhibition, of the reporter activity.

Having demonstrated that iPTH increases the binding of NFATs and SMADs to the Wnt10b promoter, we next investigated how iPTH and Tregs regulate NFAT and SMAD signaling in CD8+ T cells. We found that iPTH increases the translocation of pSMAD2, pSMAD3, NFAT1 and NFAT2 into the nucleus of BM CD8+ T cells **(figure 6A**). Blockade of Treg numeric increase by treatment with anti-CD25 Ab prevented the iPTH-induced nuclear translocation of pSMAD2, pSMAD3, NFAT1 and NFAT2 **(figure 6A**), confirming that Tregs play a pivotal role in activating NFAT and SMAD signaling in CD8+ T cells.

While NFAT signaling is known to be activated by PPR signaling (Huang et al., 2010), SMAD2/3 signaling is induced by TGFβ. PTH increases the osteoblastic production of TGFβ,

but it is possible that PTH might also increase TGFβ production by Tregs. Tregs express LAP-associated TGFβ (LAP+ TGFβ) and secrete TGFβ (Schmidt, Oberle et al., 2012, Shevach, 2009). Analysis by flow cytometry revealed that iPTH increases the relative and absolute number of LAP+ Tregs (TCRβ+CD4+Foxp3+LAP+ cells) **(figure 6B,C**). As expected, treatment with anti-CD25 Ab markedly lowered the number of LAP+ Tregs and prevented the increase in LAP+ Tregs induced by iPTH **(figure 6B,C**). Treatment with anti-CD25 Ab also prevented iPTH from upregulating the production of TGFβ1 protein levels by CD4+ cells **(figure 6D)**. Studies using FACS sorted BM Tregs from vehicle and iPTH treated Foxp3.eGFP reporter mice, established that iPTH treatment increases TGFβ1 mRNA levels in Tregs (CD4+eGFP+ cells) **(figure 6E**). Expression of TGFβ1 mRNA by purified BM cells populations is shown in **figure 6F**. Together, these data demonstrate that a consequence of the numeric increase in BM Tregs induced by iPTH is an increase in the amount of TGFβ available for upregulating nuclear pSMAD levels in CD8+ T cells. While iPTH increases the differentiation of naïve CD4+ cells into TGFβ-expressing Tregs, iPTH did not increase the Treg expression of IL-10, IL-12 and Ebi3, the two subunits of IL-35 (**Supplemental figure 8**).

To determine whether Treg-produced TGFβ is sufficient to activate SMAD signaling in CD8+ T cells, OVA specific CD8+ T cells were purified from the spleen of OT-I mice and cocultured with OVA peptide pulsed CD11c+ DCs with and without Tregs for 2 hours. Analysis of pSMAD2 and pSMAD3 in CD8+ T cells by western blotting revealed that the addition of Tregs to the cocultures resulted in increased translocation of pSMAD2 and pSMAD3 to the nucleus of CD8+ T cells **(figure 6G**). By contrast, Tregs did not upregulated the translocation of NFAT1 and NFAT2, confirming that the activation of NFAT signaling is not induced directly by Tregs.

NFAT and AP-1 form high affinity complexes binding to composite DNA sites present in genes critical for T cell activation and effector cytokine production (Fehr et al., 2010, Heissmeyer et al., 2004, Macian et al., 2002). In activated T cells, which express AP-1 at high levels, AP-1 acts as

the preferred partner of NFAT. Blockade of CD28 costimulation by Tregs, lowers the production of AP-1, forcing NFAT to bind to other partners such as SMADs (Macian, 2005). In accordance with this notion, we found that Tregs lowered c-Fos and c-Jun translocation in antigen activated CD8+ T cells **(figure 6G**). Moreover, we found that in vivo iPTH treatment did not increase the nuclear levels of c-Fos and c-Jun in CD8+ T cells **(figure 6H**), while it increased the levels of NFAT1/2 and pSMADS2/3 **(figure 6A**). These findings are relevant as they suggest that iPTH treatment favors the association of NFAT with SMADs.

Next, we investigated the role of Tregs in the production of Wnt10b induced by PTH and the involved mechanisms. OT-I CD8+ T cells were cocultured with OVA peptide pulsed CD11c+ DCs with and without Tregs for 24 hours. Some groups were also stimulated with PTH for the last 4 hours of incubation. CD8+ T cells were then purified and assayed for Wnt10b mRNA expression. In these conditions, which closely mimic the behavior of Tregs in vivo, CD8+ T cells from cocultures containing Tregs expressed ~ 3-fold higher Wnt10b mRNA levels than those without Tregs (**figure 6I**), indicating that Tregs increase the baseline production of Wnt10b. Stimulation with PTH did not increase CD8+ T cell production of Wnt10b in the absence of Tregs. By contrast, PTH increased CD8+ T cell expression of Wnt10b mRNA by ~6-fold in the presence of Tregs, demonstrating that Tregs are required for PTH to induce Wnt10b production by CD8+ T cells.

Tregs suppress conventional T cell activation via several mechanisms (Shevach, 2009). One of most relevant is inhibition of CD28 signaling in conventional T cells (Wing, Onishi et al., 2008). To investigate the role of CD28 signaling, OT-I CD8+ T cells were cocultured for 24 hours with OVA peptide pulsed CD11c+ DCs and with and without CTLA-4-Ig, an inhibitor of CD28 costimulation (Najafian & Sayegh, 2000). Some groups were also stimulated with PTH for the last 30 minutes or the last 4 hours. Confirming that blockade of CD28 costimulation by Tregs lowers the production of AP-1, we found that CTLA-4Ig lowered c-Fos and c-Jun translocation in antigen activated CD8+ T cells **(figure 6J**). CTLA-4Ig without PTH downregulated the

translocation of NFAT1, NFAT2 in fully activated cells, a finding consistent with the stimulatory role of CD28 signaling in T cell activation. However, the activation of NFAT1 and NFAT2 was increased by combined treatment with CTLA-4Ig and PTH **(figure 6K**), confirming the capacity of PTH to activate NFAT signaling. Importantly, CTLA-4Ig with and without PTH did not affect the translocation of pSMAD2 and pSMAD3. In these conditions neither CTLA-4-Ig alone nor PTH alone increased Wnt10b mRNA production by CD8+ T cells **(figure 6K)**. However, stimulation with both CTLA-4Ig and PTH resulted in a ~7-fold increase in Wnt10b mRNA levels, demonstrating that blunting of CD28 signaling increases the capacity of PTH to stimulate Wnt10b production.

To further demonstrate the relevance of CD28 signaling for PTH-induced transcription of Wnt10b, we again transfected the Wnt10b-luc reporter plasmid (or empty vector) together with TK-pRL transfection control vector into primary CD8+ T cells. We found that stimulation with anti-CD3 Ab with and without anti-CD28 Ab increased Wnt10b promoter activity above baseline levels **(figure 6L**). In vitro PTH treatment further increased Wnt10b promoter activity, but only in CD8+ T cells stimulated by anti-CD3 Ab without anti-CD28 Ab. This finding provides additional support to the hypothesis that T cell receptor (TCR) activation in the absence of CD28 signaling increases the responsiveness of the Wnt10b gene to PTH. Moreover, in this experiment the NFAT inhibitor 11R-VIVIT blocked the increase in promoter activity induced by PTH, a finding demonstrating that PTH induced Wnt10b promoter activity is NFAT dependent (**figure 6L**).

Inhibition of CD28 signaling is a key mechanism by which Tregs repress conventional T cells (Wing et al., 2008). Moreover, inhibition of CD28 signaling favors the association of NFATs with SMADs by decreasing nuclear levels of AP-1. Therefore, a final set of experiments was designed to confirm that iPTH blunts CD28 signaling in CD8+ T cells and investigate the involved mechanism. We found that iPTH downregulated the level of phosphorylated PI3K (**figure 7A**) and pAKT in BM CD8+ T cells (**figure 7B,C**), which are kinases downstream of CD28. These effects of iPTH were prevented by treatment with anti-CD25 Ab, confirming that

the increase in the number of Tregs induced by iPTH blunts CD28 signaling in CD8+ T cells. An established mechanism by which Tregs blunt CD28 signaling in conventional T cells is the downregulation of the expression of the CD28 ligands CD80/86 (B71/B72) by DCs (Shevach, 2009). Attesting to the involvement of this mechanism, we found that iPTH decreased the relative and absolute number of CD80+ mature DCs (CD11c+MHC-II+CD40+CD80+ cells) (**figure 7D,E)** and the relative and absolute number of CD86+mature DCs (CD11c+MHC-II+CD40+CD86+ cells) (**figure 7 F,G**).

DISCUSSION

iPTH treatment is an approved bone anabolic treatment for osteoporosis but its intricate mechanism of action remains largely unknown. We report (**figure 8**) that in vivo iPTH treatment increases the number of BM Tregs in mice. The increase of the BM Treg pool is essential for the bone anabolic activity of iPTH. The increase in the number of Tregs is due to enhanced differentiation of peripherally induced Tregs, a phenomenon driven by the capacity of iPTH to upregulate the levels of TGFβ and IGF-1 in the BM and to increase the sensitivity of naïve CD4+ cells to TGFβ. The numeric increase in Tregs lessens CD28 signaling in conventional BM CD8+ T cells. Stimulation of CD8+ T cells by iPTH in conditions of blunted CD28 signaling results in the binding of NFAT1/2 and SMAD3 proteins to the Wnt10b promoter and activation of Wnt10b gene expression. This Wnt ligand is required for iPTH to induce trabecular bone anabolism (Bedi et al., 2012, Li et al., 2014, Terauchi et al., 2009). To translate our findings in humans, we measured the absolute and relative frequency of Tregs in the peripheral blood of osteoporotic women treated with Teriparatide, a form of iPTH treatment. We found that Teriparatide increases the number of Tregs at 3 and 6 months of treatment. Teriparatide also increases TGFβ1 mRNA levels, an indicator of Treg activity. By, contrast, we found that in vitro treatment of Tregs with PTH does not affect the number of Tregs and TGFβ production, indicating that iPTH regulates human Tregs indirectly.

Tregs are a suppressive population of predominantly CD4+ T cells that play a critical role in maintaining immune tolerance and immune homeostasis. Accordingly, defects in Treg numbers and/or activity have been implicated in several chronic inflammatory diseases. Tregs are also know to regulate osteoclast formation (Kelchtermans et al., 2009, Kim et al., 2007, Zaiss et al., 2007), blunt bone resorption (Kim et al., 2007, Yuan et al., 2010), and prevent ovariectomy induced bone loss (Zaiss et al., 2010). However, CD4+Foxp3+ Tregs have not been previously

reported to stimulate bone formation, and iPTH treatment was not known to regulate the number of BM Tregs.

Our findings demonstrate that one mechanism by which iPTH expands murine BM Tregs is enhanced differentiation of peripherally induced Tregs. We also found iPTH not to alter Treg proliferation and homing to the BM. Whether additional mechanisms, such as increased life-span contribute to the numeric increase of BM Tregs remains to be determined.

PPR is expressed by conventional CD4+ cells and CD8+ cells but not by Tregs. On the other hand, iPTH upregulates the BM levels of TGFβ and IGF-1, factor capable of inducing Treg differentiation in vitro (Anguela et al., 2013, Chen et al., 2003, Johannesson et al., 2014, Liu et al., 2008, Ohkura et al., 2013). Therefore, iPTH is likely to induce murine Treg differentiation indirectly.

In the mouse, iPTH treatment for 4 weeks did not increase the number of Tregs in the spleen, thymus and intestinal wall, suggesting that a treatment period longer than 4 weeks might be required for iPTH to expand Tregs in peripheral blood and lymphoid organs, a hypothesis supported by our findings in humans at 3 and 6 months of treatment. It is also likely that the increase in Tregs induced by iPTH occurs first in the BM because of environmental cues. iPTH increases the osteoblastic production of TGFβ and the bone matrix is the largest reservoir of TGFβ in the body (Koh, Novince et al., 2011, Pfeilschifter et al., 1995). iPTH also increases the osteoblastic production of IGF-1 (McCarthy et al., 1989, Pfeilschifter et al., 1995). It is thus likely that in the first 4 weeks of treatment the increase in the number of Tregs induced by iPTH is confined to the BM because of the higher levels of TGFβ and IGF-1 present in the BM as compared to the spleen.

We have used two experimental models to assess the relevance of Tregs for the anabolic activity of iPTH in the mouse, depletion of Tregs in WT mice by treatment with anti-CD25 Ab, and depletion of Tregs in DEREG mice by treatment with DT. Both strategies prevented the

increase in the number of Tregs induced by iPTH. In both cases, blockade of the increase in the number of Tregs prevented the increases in bone formation and trabecular bone volume induced by iPTH, demonstrating that an enlargement of the pool of BM Tregs is required for iPTH to increase trabecular bone mass. Blockade of the increase in the number of Tregs also prevented the increase in Wnt10b production induced by iPTH. This Wnt ligand is required for iPTH to induce bone anabolism (Bedi et al., 2012, Li et al., 2014, Terauchi et al., 2009). Accordingly, blockade of Tregs and silencing of Wnt10b production by CD8+ T cells (Bedi et al., 2012, Terauchi et al., 2009) equally blunt the anabolic activity of iPTH in trabecular bone. By contrast, blockade of Tregs did not blunt the capacity of iPTH to increase cortical bone volume. These findings are in agreement with previous reports from our laboratory demonstrating that T cells and Wnt10b do not contribute to iPTH-induced cortical bone anabolism (Bedi et al., 2012, Li et al., 2014, Terauchi et al., 2009). We hypothesize that iPTH induces cortical bone anabolism primarily by regulating the osteocytic production of sclerostin.

The Wnt10b promoter possesses 3 DNA monomeric core motifs for NFAT binding in close proximity to SMAD binding sites. We found one of these binding sites, located between -705 bp and -272 bp in the Wnt10b promoter, to be critical for the Wnt10b transcription induced by IPTH.

The NFAT family of transcription factors includes 5 members, NFAT1 to 5, of which NFAT1 (NFATc2) and NFAT2 (NFATc1) play a central role in CD4+ and CD8+ T cell activation, tolerance, anergy and exhaustion (Fehr et al., 2010, Heissmeyer et al., 2004, Macian et al., 2002). Activation of calcineurin upon TCR signaling leads to dephosphorylation of NFATs, which then translocate to the nucleus where they activate transcription by interacting with AP-1 and other nuclear proteins (Macian, 2005). We found that iPTH treatment upregulates the nuclear translocation of NFAT1/2 and SMAD2/3 and the binding of NFAT1/2 and SMAD3 to the Wnt10b promoter in BM CD8+ T cells. As previously reported for other promoters (Dichlberger, Schlager et al., 2014, Tone, Furuuchi et al., 2008), SMAD2 did not cooperate with NFAT to induce Wnt10b expression.

Tregs express high levels of membrane-bound and soluble TGFβ (25, 57). We found iPTH treatment to increase the expression of membrane bound TGFβ by Tregs and partial Treg depletion by treatment with anti-CD25 Ab to block the increase the nuclear levels of SMAD2 and SMAD3 induced by iPTH. It is thus likely that increased expression of membrane bound TGFβ by Tregs provides iPTH with a mechanism to activate SMAD signaling in CD8+ T cells in close proximity to Tregs. Tregs are highly mobile cells, therefore even a relative low number of TGFβ+ Tregs may activate SMAD signaling in many CD8+ cells. Moreover, it appears likely that PTH induces NFAT translocation by directly targeting CD8+ T cells, as PTH and PTHrP have been previously shown to directly activate NFAT signaling in other cell lineages (Huang et al., 2010, Park et al., 2015). Importantly, since blockade of Tregs dampens the translocation of NFAT to the nucleus of CD8+ T cells, NFAT activation by iPTH requires signals conveyed to CD8+ T cells by an enlarged population of Tregs. However, we cannot conclusively exclude the possibility that iPTH activates NFAT signaling in CD8+ T cells via a non-cell autonomous effect mediated by Tregs.

Tregs suppress conventional T cell activation through a multitude of mechanisms (Shevach, 2009), including the blunting of CD28 signaling in CD8+ T cells (Wing et al., 2008). Accordingly, we found that iPTH lessen CD80/CD86 expression on antigen presenting cells, thereby reducing CD28 signaling in conventional BM CD8+ T cells. CD28 signaling is relevant for regulating the association of NFAT to its partners because it leads to the activation of AP-1, which is the preferred partner of NFAT (Fehr et al., 2010, Heissmeyer et al., 2004, Macian et al., 2002). As a result, in the context of T cell activation, NFAT and AP-1 form high affinity complexes binding to composite DNA sites present in genes critical for T cell activation and effector cytokine production (Fehr et al., 2010, Heissmeyer et al., 2004, Macian et al., 2002). Blockade of CD28 costimulation by Tregs, lowers the production of AP-1, favoring the binding of NFAT to other partners, such as SMADs (Macian, 2005).

In this study, we found evidence in support of the relevance of CD28 signaling blockade for the increase in Wnt10b gene expression induced by iPTH. This evidence includes in vitro studies demonstrating that antibody-induced activation of CD28 blocks the capacity of PTH to activate Wnt10b gene expression. Conversely, blockade of CD28 signaling in vitro by CTLA-4Ig results in higher production of Wnt10b. Attesting to the relevance of repression of CD28 signaling for Wnt10b production in vivo, we have reported that in vivo inhibition of CD28 signaling via treatment with CTLA-4Ig increases expression of Wnt10b by CD8+ T cells and bone mass in a manner similar to iPTH (Roser-Page, Vikulina et al., 2014). Therefore, iPTH favors the formation of lower affinity complexes between NFAT1/2 and SMAD3, which bind to the Wnt10b promoter and stimulation of Wnt10 transcription.

Recently, there has been an explosion in research investigating the potential to manipulate Tregs for clinical purposes (Brunstein, Miller et al., 2011, Di Ianni, Falzetti et al., 2011, Feng, Hu et al., 2013, Marek-Trzonkowska, Mysliwiec et al., 2012, Trzonkowski, Bieniaszewska et al., 2009). Among these studies are several phase I clinical trials to test whether boosting Treg numbers and/or function is a feasible, safe, and potentially effective way to treat diseases such as graft vs. host disease, type 1 diabetes and to prevent the rejection of transplanted organs (Brunstein et al., 2011, Di Ianni et al., 2011, Feng et al., 2013, Marek-Trzonkowska et al., 2012, Trzonkowski et al., 2009). Osteoporosis is a common chronic disorder that represents a major source of disability in the elderly. Novel anabolic treatments are needed because the long-term use of current antiresorptive agents is associated with significant adverse events and complications. An increase in the number of Treg is achievable by Treg transfer or treatment with mTOR inhibitors, self-antigens or cytokines (von Boehmer & Daniel, 2013), and inhibition of CD28 costimulation (e.g. CTLA-4Ig). Based on our findings, pharmacological Tregs may represent a novel therapeutic modality for osteoporosis or for potentiating the anabolic activity of iPTH. Moreover, the use of iPTH to increase the number of Tregs may find applications in transplant medicine or as a treatment for inflammatory and autoimmune conditions.

AUTHOR CONTRIBUTIONS: MY, RDP, MNW, and RP designed the animal studies. PDA, FS and IB designed and performed the human studies and analyzed the human data. MY, CV, AMT, JYL, EH, JA and MS performed the research and analyzed the animal data. RP wrote the manuscript.

ACKNOWLEDGEMENTS

This study was supported by grants from the National Institutes of Health (RP:DK108842, AR54625, and RR028009; JYL: AR061453; MNW: AG040013, AR068157 and AR070091). MNW was also supported by a grant from the Biomedical Laboratory Research & Development Service of the VA Office of Research and Development (5I01BX000105).

MATERIAL AND METHODS

Human Study population. All human studies were approved by the Ethical Committee of the A.O.U. Città della Salute e della Scienza - A.O. Ordine Mauriziano - A.S.L. TO1, Turin Italy and informed consent was obtained from all participants. The study population was recruited from the patients of A.O.U. Città della Salute e della Scienza, Turin Italy. The study population included 34 women affected by postmenopausal osteoporosis (PMO). The demographic characteristics of the study population are shown in table 1. The diagnosis of PMO was established based on WHO criteria (1984) the presence of secondary osteoporosis was ruled out by medical history, physic examination and blood exams quantifying calcium, phosphorus, 25OH vitamin D and PTH. Inclusion and exclusion criteria are provided in supplemental experimental procedures. Seventeen patients were treated with calcium carbonate (1000 mg/day) and colecalcipherol 800 UI/day (control treatment). The remaining seventeen patients were treated with human PTH 1-34 (Teriparatide, Eli Lilli, Indianapolis) 20 μg/day subcutaneously, calcium carbonate (1000 mg/day) and colecalcipherol 800 UI/day. Patients in the Teriparatide group had prior fragility fractures, whereas those in the control treatment group had not, according to guide lines for PMO treatment of the Italian Health ministry. Blood samples (40 ml) were collected in EDTA containing vacuum tubes at baseline and after 3 and 6 months of treatment. Exclusion criteria are provided in supplemental information.

Study design. No randomization procedure was used to assign humans and mice to experimental groups. All murine and human samples were analyzed in blinded fashion. The Investigators analyzing the human samples were blind to the identity of the study participant, disease state, treatment status and all other clinical variables. The Investigators analyzing mouse samples were blind the genotype and treatment group. Congenic WT mice or non-transgenic littermates were used as controls for transgenic mice.

Inclusion and eexclusion criteria for the human study population.

None of the subjects enrolled were affected by disease states affecting bone health other than PMO. Subjects affected by renal or hepatic insufficiency or chronic inflammatory conditions such as rheumatoid arthritis, psoriasis, and inflammatory bowel disease were excluded, as these diseases are known to influence bone status. Subjects treated with drugs active on bone turnover such as bisphosphonates, denosumab, teriparatide, hormone replacement therapy, selective estrogen receptor modulator, strontium ranelate, glucocorticoids, androgens or GN-RH agonists for any length of time during the 6 months prior to enrolment were excluded.

Flow cytometric analysis of human samples. Peripheral blood mononuclear cells (PBMCs) were purified from 40 ml peripheral blood obtained from all patients at each time point using the Ficoll–Paque gradient method, as previously described (D'Amelio, Grimaldi et al., 2005). The Human Regulatory T-cell Staining Kit (eBioscience Inc. San Diego, CA, USA) was used in accordance with manufacturer's instructions to stain PBMC for Tregs. Briefly, the following labelled monoclonal antibodies and corresponding isotype controls were used: anti-CD4 (FITC-conjugated); anti-CD25 (APC-conjugated); and anti-Foxp3 (PE-conjugated). After surface staining for CD4 and CD25, cells were washed, fixed and permeabilized (Fix-Perm Buffer). Cells were then incubated with anti-Foxp3 for intra-nuclear staining. Flow cytometry was performed on an Accuri C6 flow cytometer (BD Biosciences).

Human T cells immunomagnetic separation. Human CD4+CD25+ T cells were isolated from whole blood at each time point using The Complete Kit for Human CD4+CD25+ Regulatory T Cells which includes RosetteSep CD4+ T Cell Enrichment Cocktail and EasySep Human CD25 Positive Selection Kit (STEMCELL Technologies) according to the manufacturer instructions. The purity of CD4+CD25+ T cells was 93-95 % as assessed by flow cytometry.

Real-time RT-PCR and human primers. RT-PCR was used to evaluate the mRNA levels of TGFβ1 in CD4+CD25+ T cells. RNA was isolated using TRIzol reagent (Ambion, Huntingdon, UK), according to the manufacturer's protocol. 1 μg of RNA was reverse transcribed to single-

stranded cDNA using the High Capacity cDNA Reverse Transcription Kit (Applied-Biosystems). RT-PCR was performed with IQ SYBR Green Supermix (BIORAD). The housekeeping control gene was β-Actin and gene expression was quantified using the $2^{-\Delta\Delta Ct}$ method. The primers used were as follows: 5'-CTCTCCGACCTGCCACAGA-3' (forward) and 3'-TCTCAGTATCCCACGGAAATAACC-5' (reverse) for TGFβ1; 5'-CCTAAAAGCCACCCCACTTCT -3' (forward) and 3'- CACCTCCCCTGTGTGGACTT -5' (reverse) for β-Actin.

In vitro PTH treatment of human CD4+CD25+ T cells. Purified CD4+CD25+ T cells were cultured for 6 days in RPMI medium containing 10% fetal bovine serum (FBS), 1% Penicillin Streptomycin (Gibco, Thermo Fisher Scientific, MA, USA), 500U/ml rIL-2 (Tebu-bio srl, Milano, ITALY) and 2 μg/ml anti-CD3 antibody (Biolegend, San Diego, CA, USA) and cultured for 16h in the absence of PTH 1-34. Human PTH 1-34 (50 ng/ml) or control vehicle was added to the cultures for 1 hour or 24 hours for 3 times during the 6-days culture to mimic the anabolic effects of intermittent PTH 1-34. Cells were then harvested and utilized for flow cytometry and RNA extraction.

Animals. All the animal procedures were approved by the Institutional Animal Care and Use Committee of Emory University. All in vivo experiments were carried out in female mice. In vitro experiments were conducted using primary cells from female mice or EL4 cells. Female C57BL/6 WT, TCRβ-/-, DEREG and Foxp3 eGFP knock-in mice were purchased from Jackson Laboratories (Bar Harbor, ME). All mice were maintained under specific pathogen free conditions and fed sterilized food (5V5R chow) and autoclaved water ad libitum.

In vivo iPTH treatment. For the in vivo iPTH studies, 80 μg/kg/day of hPTH 1-34 (Bachem California Inc., Torrance, CA) or vehicle was injected daily subcutaneously into female mice for 1-4 weeks starting at the age of 6 weeks, as described (Bedi et al., 2012, Li, Adams et al., 2012, Li et al., 2014, Terauchi et al., 2009).

T cell purification and adoptive transfer. Splenic T cells from 6-8 weeks old Foxp3 eGFP knock in mice were enriched by negative selection using EasySep Mouse T Cell Isolation Kit (StemCell Technologies, Auburn, CA). Next, conventional CD4+ T cells (CD4+eGFP-) were purified from enriched splenic T cells by FACS sorting and transferred into 4 weeks old TCRβ-/- recipient mice by IV injection (3×10^6 cells per mouse). Recipient mice were treated with vehicle or iPTH for 1-4 weeks starting 2 weeks after the CD4+eGFP- cell transfer. For Treg isolation, CD4+eGFP+ cells were sorted from enriched splenic T cells of Foxp3 eGFP knock in mice and injected into 6 weeks old TCRβ-/- recipient mice via tail vein (2×10^6 cells per mouse). The purity of CD4+eGFP+ cells was 99 % checked by flow cytometry. Vehicle or iPTH treatment were started the day of the Treg transfer for 2 weeks. At the end of the treatment period, the number of CD4+eGFP+ cells was determined by flow cytometry in spleen and BM cells.

Small intestine Lamina propria lymphocyte (SILP) isolation. Lamina propria lymphocyte isolation was performed as described (Li, Chassaing et al., 2016). Briefly, the small intestine was removed and flushed of fecal contents, and intestinal segments containing Peyer's patches were excised. The intestine was opened longitudinally and cut into 5 mm pieces. Tissues were transferred into a 50 ml conical tube, and shaken at 250 rpm for 20 min at 37°C in HBSS medium (Life Technologies, Grand Island, NY) supplemented with 5% FBS (Mediatech Inc., Manassas, VA) containing 2 mM EDTA. This process was repeated two additional times. The tissue suspension was passed through a strainer, and the remaining intestinal tissue was washed and then minced, transferred into a fresh 50 ml conical tube, and shaken for 20 min at 37°C in HBSS + 5% FBS containing type VIII collagenase (Sigma-Aldrich, St. Louis, MO) at 1.5 mg/ml. The tissue suspension was collected, passed through a strainer, and pelleted by centrifugation at 1200 rpm for 3 min. The pellet was suspended in 10 ml HBSS medium and passed through glass wool halfway packed in a 10 ml syringe to remove undigested tissue pieces. The cell suspension was collected in a 50 ml tube and centrifuged at 1200 rpm for 3 min. The pellet was suspended in 5 ml HBSS and 5 ml 90% isotonic Percoll, and then

transferred into a 15 ml tube and mixed by tilting back and forth. The cell content was layered onto 2 ml of 70% isotonic Percoll. The gradient was centrifuged at 2000 rpm for 20 min. Cells were collected from the interface area and washed by centrifugation in 10 ml supplemented RPMI-1640 medium supplemented with 5% FBS. The cell pellet was resuspended in 10 ml supplemented RPMI-1640 and cell number was counted.

Anti-CD25 Ab treatment. 6-week-old WT mice were injected daily with vehicle or PTH for 4 weeks (day 1 to 28). Mice were also injected with anti-CD25 Ab (clone PC61, 500 μg/mouse/injection IP) (BioXCell, West Lebanon, NH) on days -2, 0, 5 and 7 or isotype matched irrelevant Ab.

DT treatment. DT was purchased from Merck (catalog number 322326), and each lot was tested for toxicity in WT mice and titrated for potency in DEREG mice prior to use. DEREG and littermate control mice were administered 1 μg DT intraperitoneally on two consecutive days each week for total four weeks.

μCT measurements. μCT scanning and analysis of the distal femur was performed as reported previously (Li, D'Amelio et al., 2015, Li et al., 2014, Robinson, Li et al., 2015) using a Scanco μCT-40 scanner (Scanco Medical, Bassersdorf, Switzerland).

Femoral trabecular and cortical bone regions were evaluated using isotropic 12-μm voxels. For the femoral trabecular region we analyzed 140 slices from the 50 slices under the distal growth plate. Femoral cortical bone was assessed using 80 continuous CT slides located at the femoral midshaft. X-ray tube potential was 70 kVp, and integration time was 200ms.

Quantitative bone histomorphometry. The measurements, terminology and units used for histomorphometric analysis, were those recommended by the Nomenclature Committee of the American Society of Bone and Mineral Research (Dempster, Compston et al., 2013). Non-consecutive longitudinal sections of the femur were prepared and analyzed as described previously (Li et al., 2015). Mice were injected subcutaneously with calcein at day 7 and day 2

before sacrifice. Non-consecutive longitudinal sections (5 μm thick) were cut from methyl methacrylate plastic-embedded blocks along the frontal plane using a Leica RM2155 microtome and were stained with Goldner's trichrome stain for the static measurements. Additional sections were cut at 10 μm, and left unstained for dynamic (fluorescent) measurements. Measurements were obtained in an area of cancellous bone that measured ≈ 2.5 mm^2 and contained only secondary spongiosa, which was located 0.5–2.5 mm proximal to the epiphyseal growth cartilage of the femurs. Measurements of single-labeled and double-labeled fluorescent surfaces, and interlabel width were made in the same region of interest using unstained sections. Mineral Apposition Rate (MAR) and Bone Formation Rate (BFR) were calculated by the software by applying the interlabel period. Histomorphometry was done using the Bioquant Image Analysis System (R&M Biometrics).

Markers of bone turnover. Serum CTX and osteocalcin were measured by rodent specific ELISA assays (Immunodiagnostic Systems, Scottsdale, AZ).

Stromal cells purification. BM SCs were purified as previously described (Bedi et al., 2012, Li et al., 2014, Terauchi et al., 2009). In brief, BM cells from long bones were cultured for 7 days in α-MEM medium containing 10% FBS, 100 mg/mL of penicillin, and 100 IU/mL of streptomycin, to allow the proliferation of SCs. After removing non adherent cells, adherent macrophages were eliminated by positive immunoselection using anti-CD11c MACS Microbeads (Miltenyi Biotech, Auburn, CA, USA). The remaining adherent cells were defined as SCs as they express alkaline phosphatase (ALP), type-I collagen, and Runx2, and have the capacity to form mineralization nodules when further cultured under mineralizing conditions.

BrdU incorporation studies. Mice were injected IP with 40 mg/kg/day of BrdU solution for four days and sacrificed 24 hours later. BrdU detection was performed by using the BrdU Flow Kit (BD Biosciences, San Diego, CA) and analyzing cells by flow cytometry. The percentage of BrdU+ Treg cells was quantified by gating CD4+Foxp3+ cells in the TCRβ+ cell population.

SC Thymidine incorporation assay. The proliferation of purified SCs was measured by [3H]-thymidine incorporation assay. SCs were pulsed with [3H]-thymidine (0.5 μCi/10,000 cells) for 18 hours, and were harvested with a Cell Harvestor (Skatron, Inc., Sterling, VA, USA). [3H]-thymidine incorporation was read by a LS 6000 IC Liquid Scintillation Counter (Beckman Coulter, Inc., Fullerton, CA, USA).

SC apoptosis assay. The activity of caspase-3, the critical protease in the induction of apoptosis, was measured in SCs using CaspACE Assay System (Promega Corporation, Madison, WI, USA) according to the manufacturer's protocol.

In vitro Treg differentiation. Assessment of Treg differentiation in vitro was carried out as described (Fantini, Dominitzki et al., 2007). Splenic CD4+ T cells from WT mice treated with vehicle or iPTH were purified by negative selection using EasySep Mouse CD4+ T Cell Isolation Kit (StemCell Technologies, Auburn, CA). CD25+ cells were then removed using the EasySep Mouse CD25 Regulatory T Cell Positive Isolation Kit (StemCell Technologies, Auburn, CA). The remaining cells (CD25- enriched CD4+ T cells) were cultured in plates coated with anti-CD3 Ab (3 μg/ml) in the presence of anti-CD28 Ab (3 μg/ml), IL-2 (5 ng/ml), and TGFβ1 (0.1-5 ng/ml) for 3 days. Cells were then harvested and analyzed by flow cytometry to enumerate CD4+Foxp3+ cells.

In vitro generation of induced Tregs. The generation was carried out as described (Karlsson et al., 2011) . Briefly, purified splenic CD4+CD25- T cells from WT mice at the concentration of one million each ml completed RPMI-1640 medium were cultured in plates coated with anti-CD3 Ab (10 μg/ml) in the presence of recombinant human IL-2 (100 U/ml), TGFβ1 (20 ng/ml) and all trans retinoic acid (1 pmol/ml) for 4 days. The conversion ratio of cells reached 95 % (the percentage of Foxp3+ cells in total CD4+ population).

Flow cytometry. Flow cytometry was performed on a LSR II system (BD Biosciences, Franklin Lakes, NJ) and data were analyzed using FlowJo software (Tree Star, Inc., Ashland, OR). For intracellular Foxp3 staining, APC-Foxp3 (eBioscience) antibody was added after cell

fixation and permeabilization with BD Transcription Factor Buffer Set (BD Biosciences). For phospho-epitope analysis, resting total BM cells were fixed with BD Cytofix Fixation Buffer for 10 min at 37°C, permeabilized in BD Phosflow Perm Buffer III for 30 min on ice, and stained with PE anti-AKT (pS473) (BD Biosciences). The antibodies used for cell surface staining are provided as supplemental information. The following anti-mouse antibodies were used for cell surface staining: purified CD16/32, BV 421-TCRβ, PerCP/Cy5.5-CD4, PE-CD25, BV 711-CD8, FITC-B220, APC/Cy7-CD3, PerCP/Cy5.5-F4/80, BV 421-CD11c, Alexa Fluor 700-I-A/I-E, PE-CD40, APC-CD80, PE-LAP(Biolegend, San Diego, CA) and BV650-CD86 (BD Biosciences).

Real-time RT-PCR and murine primers. WT BM CD8+ T cells were enriched using EasySep Mouse CD8a positive Selection Kit II (StemCell Technologies, Auburn, CA) while WT spleen CD8+ T cells were purified by negative selection with EasySep Mouse CD8+ T Cell Isolation Kit (StemCell Technologies, Auburn, CA). BM TCRβ+CD4+eGFP- , TCRβ+CD4+eGFP+ (Treg) and TCRβ+CD8+ T cells from Foxp3 eGFP knock in mice were FACS sorted by FACS ARIA II. Total RNA was isolated from WT cells including total BM cells, splenic CD8+ T cells or BM CD8+ T cells using TRIzol reagent (ThermoFisher Scientific). FACS Sorted cells were lysed using the Cells-to-cDNA II Kit (ThermoFisher Scientific). For all RNA samples, cDNA was synthesized with random hexamer primers (Roche) and AMV reverse transcriptase (Roche). mRNAs levels of murine Wnt10b and TGFβ1 in T cells, that of bone sialoprotein (BSP), collagen 1 (CoL1), osteocalcin (Ocn), osterix (Osx) and runt-related transcription factor 2 (Runx2) in SCs and that of TNF, IL-6, IFNγ, IL-4, IL-13 and IL-17A in total BM were quantified by real-time PCR. . Changes in relative gene expression between vehicle and iPTH groups were calculated using the $2^{-\Delta\Delta CT}$ method with normalization to 18S rRNA. The primers used are provided in supplemental Table 1.

TGF-β1 and IGF-1 ELISA BM cells from long bones were cultured for 24 hr. Supernatants were collected and assayed for TGF-β1 or IGF-1 by ELISA kits (R&D Systems) following the manufacturer's instruction. When checking TGF-β1, the medium without the cells was run as the

control of the baseline levels of TGF-β1. To isolate CD4+ T cells from BM, BM CD8+ T cells were discarded by EasySep Mouse CD8a positive Selection Kit II (StemCell Technologies). CD4+ T cells were then positively isolated using APC-anti-TCRβ antibody and EasySep Mouse APC Positive Selection Kit (StemCell Technologies).

Western Blotting. The nuclear and cytoplasmic fractionations of fresh BM CD8+ T cells were obtained using NE-PER Nuclear and Cytoplasmic Extraction Reagents (ThermoFisher Scientific). Halt Protease and Phosphatase Inhibitor Cocktail (ThermoFisher Scientific) were added into the reagents before using. Lysates were cleared by centrifugation and the supernatants were boiled in SDS loading buffer. The same amount of proteins was separated on 10% Mini-PROTEAN TGX Precast Gels (Bio-rad) and electroblotted to nitrocellulose membrane (ThermoFisher Scientific). Proteins were detected by anti-NFAT1, anti-c-Jun (ThermoFisher Scientific), anti-NFAT2, anti-c-Fos (Santa Cruz Biotechnology), anti-phospho-Smad2 (Ser465/467) or anti-phospho-Smad3 (Ser423/425) antibody (Cell Signaling Technology, Danvers, MA)/anti-Smad3 (phosphor S423+ S425) (Abcam). Anti-beta Tubulin (Abcam) and anti-Lamin B1 (Cell Signaling Technology, Danvers, MA) antibodies were used to confirm the purity of subcellular fractionations, respectively. Anti-beta actin antibody was bought from Santa Cruz Biotechnology and used as the loading control for the testing of Smad7 (Santa Cruz Biotechnology), phospho-Smad2 (Ser465/467) and phospho-Smad3 (Ser423/425) (Cell Signaling Technology, Danvers, MA) in the whole lysate from splenic conventional CD4+ T cells or phospho-PI3K p85 (Cell Signaling Technology, Danvers, MA) in the whole lysate from BM CD8+ T cells. Western blot analysis was conducted by using Luminata Crescendo Western HRP substrate (EMD Millipore). Band intensities were quantified with Quantity One 1D Analysis Software (Bio-Rad Laboratories) and expressed relative to Lamin B1 or beta-actin.

Plasmids and site-directed mutagenesis. The plasmid containing -2000 to +216 bp DNA sequence of mouse Wnt10b promoter was constructed by inserting a PCR product of mouse genomic DNA into the pGL3.0 vector (Promega, Madison, WI). mWnt10b-luc (-705 to +216 bp)

is a gift from Dr. D. J. Klemm, University of Colorado, Denver. Other shortened constructs were subcloned basing on the construct of mWnt10b-luc (-2000 bp to +216 bp). The amplification template for all mutations is the mWnt10b-luc (-705 to +216 bp). The NFAT binding site (5'-AGGAAAA-3') at -282 to -276 bp was changed to 5'-AGcttAA-3' using the Q5 Site-Directed Mutagenesis Kit (New England BioLabs). Similarly, the SMAD binding site (5'-GTCTAGA-3') at -341 to -335 bp was mutated to 5'-catagcg-3'. The primers used are provided in supplemental Table 1.

Wnt10b promoter reporter gene assays. EL4 cell line bought from ATCC (ATCC number: TIB-39 and lot number: 61840715). EL4 cells were negative for mycoplasma contamination according to the Hoechst DNA method and agar culture method. The cells were transfected with either 1.8 μg pGL3 basic vector or 1.8 μg mWnt10b-luc reporter construct together with 0.2 μg TK-pRL control vector using the Amaxa Nucleofector system and Amaxa Cell Line Nucleofector Kit L (Lonza). For primary cells, freshly purified spleen CD8+ T cells were transfected with either 3.6 μg pGL3 basic vector or 3.6 μg mWnt10b-luc reporter construct together with 0.4 μg TK-pRL control vector using the Amaxa Nucleofector system and Amaxa Mouse T Cell Nucleofector Kit (Lonza). Cells were left unstimulating for 24 h and cultured with ionomycin (0.5 μg/ml, Sigma) plus TGFβ1 (5 ng/ml, Biolegend) for another 24 h. In some experiments, unstimulated, anti-CD3 Ab or anti-CD3/CD28 Ab stimulated cells were transfected with constructs separately. Transfected cells were left unstimulated for 24 h or treated with 4 μM 11R-VIVIT (Merck Millipore) and/or 50 nM PTH(1-34) after 22 h for the last 2 h. Luciferase activity was determined by the Dual-Luciferase reporter assay kit (Promega BioSciences, San Luis Obispo, CA).

ChIPs. Chromatin immunoprecipitation (ChIP) assays were performed using Pierce Agarose ChIP Kit (ThermoFisher Scientific) and following the detailed manufacturer's instructions. Fresh purified BM CD8+ T cells were fixed in 1% formaldehyde for 10 minutes. Chromatin was digested by micrococcal nuclease to an average length of 200-1000 bp. The similar amounts of

chromatin were immunoprecipitated with 2 μg of anti-NFAT1 (MA1-025, ThermoFisher Scientific), anti-NFAT2 (7A6, Santa Cruz Biotechnology), anti-Smad3 (ChIP grade, Abcam), anti-Smad2 (Cell Signaling Technology, Danvers, MA) or control rabbit IgG. Isolated DNAs were quantitated using ABI SYBR Green PCR master mix (Applied Biosystems) on an ABI StepOnePlus Real-Time PCR System and calculated as fold enrichment compared with background signal. The primers used are provided in Supplemental Table 1.

APC assay and in vitro CTLA-4Ig treatment. The assay was performed as previously described (Roser-Page et al., 2014). Additional information is provided as supplemental information. Splenic CD11c+ dendritic cells (DCs) sorted by immunomagnetic beads (Miltenyi Biotech) were used as antigen presenting cells. CD8+ T cells expressing a monoclonal ovalbumin (OVA)-specific transgenic TCR were purified from the spleens of OT-I mice by negative selection. CD11c+ DCs were pulsed for 4 hours with 1 μM antigen (OVA peptide) (SIINFEKL, InvivoGen). After two time washes with medium, cells were ready for APC assay. For induced Treg coculture, OVA presenting dendritic cells at 150,000/well were incubated with splenic OT-I CD8+ T cells (1 million/well) with or without induced Tregs (1million/well) for 24 h and with or without hPTH 1-34 (100nM) (Bachem California Inc., Torrance, CA) at last 4 h. CD8+ T cells were separated by positive selection beads and dissolved in TRIzol reagent for RNA isolation and Wnt10b mRNA level assay by real time RT-PCR. For western blotting, the time of coculture of OVA presenting dendritic cells, CD8+ T cells and induced Tregs was 2 h. During CTLA-4-Ig treatment, OVA presenting dendritic cells at 150,000/well were incubated with splenic OT-I CD8+ T cells (1 million/well) with or without CTLA-4-Ig (100 μg/ml) for 24 h. The treated times of PTH at final time point are 4 h for real time PCR and thirty minutes for western blotting

Statistical Analysis. Human Tregs and human TGFβ1 data were analyzed by ANOVA for repeated measures. Human demographic and clinical data were analyzed by unpaired two tailed t-tests. When murine data were normally distributed according to the Shapiro-Wilk

normality test they were analyzed by unpaired two tailed t-tests, one-way or two-way analysis-of-variance, as appropriate. This analysis included the main effects for animal strain and treatment plus the statistical interaction between animal strain and treatment. When the statistical interaction between animal strain and treatment group was not statistically significant ($p > 0.05$) nor suggestive of an important interaction ($p > 0.10$), p values for the main effects tests were reported. When the statistical interaction was statistically significant ($p < 0.05$) or suggestive of an important interaction, then t tests were used to compare the differences between the treatment means for each animal strain, applying the Bonferroni correction for multiple comparisons. Data that were not normally distributed (as tested by Shapiro-Wilk normality test) were analyzed by Kruskal-Wallis non-parametric tests.

REFERENCES

(1984) Osteoporosis. National Institutes of Health Consensus Development Conference Statement. Natl Inst Health Consens Dev Conf Consens Statement 5: 6 p

Abbas AK, Benoist C, Bluestone JA, Campbell DJ, Ghosh S, Hori S, Jiang S, Kuchroo VK, Mathis D, Roncarolo MG, Rudensky A, Sakaguchi S, Shevach EM, Vignali DA, Ziegler SF (2013) Regulatory T cells: recommendations to simplify the nomenclature. Nat Immunol 14: 307-8

Anguela XM, Tafuro S, Roca C, Callejas D, Agudo J, Obach M, Ribera A, Ruzo A, Mann CJ, Casellas A, Bosch F (2013) Nonviral-mediated hepatic expression of IGF-I increases Treg levels and suppresses autoimmune diabetes in mice. Diabetes 62: 551-60

Bedi B, Li JY, Tawfeek H, Baek KH, Adams J, Vangara SS, Chang MK, Kneissel M, Weitzmann MN, Pacifici R (2012) Silencing of parathyroid hormone (PTH) receptor 1 in T cells blunts the bone anabolic activity of PTH. Proc Natl Acad Sci U S A 109: E725-33

Bellido T, Ali AA, Gubrij I, Plotkin LI, Fu Q, O'Brien CA, Manolagas SC, Jilka RL (2005) Chronic elevation of parathyroid hormone in mice reduces expression of sclerostin by osteocytes: a novel mechanism for hormonal control of osteoblastogenesis. Endocrinology 146: 4577-83

Bennett CN, Ouyang H, Ma YL, Zeng Q, Gerin I, Sousa KM, Lane TF, Krishnan V, Hankenson KD, MacDougald OA (2007) Wnt10b increases postnatal bone formation by enhancing osteoblast differentiation. J Bone Miner Res 22: 1924-32

Bertolini DR, Nedwin GE, Bringman TS, Smith DD, Mundy GR (1986) Stimulation of bone resorption and inhibition of bone formation in vitro by human tumor necrosis factor. Nature 319: 516-518

Betts RJ, Ho AW, Kemeny DM (2011) Partial depletion of natural CD4(+)CD25(+) regulatory T cells with anti-CD25 antibody does not alter the course of acute influenza A virus infection. PLoS ONE 6: e27849

Brunstein CG, Miller JS, Cao Q, McKenna DH, Hippen KL, Curtsinger J, Defor T, Levine BL, June CH, Rubinstein P, McGlave PB, Blazar BR, Wagner JE (2011) Infusion of ex vivo expanded T regulatory cells in adults transplanted with umbilical cord blood: safety profile and detection kinetics. Blood 117: 1061-70

Calvi LM, Sims NA, Hunzelman JL, Knight MC, Giovannetti A, Saxton JM, Kronenberg HM, Baron R, Schipani E (2001) Activated parathyroid hormone/parathyroid hormone-related protein receptor in osteoblastic cells differentially affects cortical and trabecular bone. J Clin Invest 107: 277-86

Chaudhry A, Rudensky AY (2013) Control of inflammation by integration of environmental cues by regulatory T cells. J Clin Invest 123: 939-44

Chen W, Jin W, Hardegen N, Lei KJ, Li L, Marinos N, McGrady G, Wahl SM (2003) Conversion of peripheral CD4+CD25- naive T cells to CD4+CD25+ regulatory T cells by TGF-beta induction of transcription factor Foxp3. J Exp Med 198: 1875-86

Cho SW, Pirih FQ, Koh AJ, Michalski M, Matt E, Ritchie K, Sinder B, Oh S, Al-Dujaili SA, Lee J, Kozloff K, Danciu T, Wronski TJ, McCauley LK (2013) The soluble interleukin-6 receptor is a mediator of hematopoietic and skeletal actions of parathyroid hormone. The Journal of biological chemistry

Cho SW, Soki FN, Koh AJ, Eber MR, Entezami P, Park SI, van Rooijen N, McCauley LK (2014) Osteal macrophages support physiologic skeletal remodeling and anabolic actions of parathyroid hormone in bone. Proc Natl Acad Sci U S A

D'Amelio P, Grimaldi A, Pescarmona GP, Tamone C, Roato I, Isaia G (2005) Spontaneous osteoclast formation from peripheral blood mononuclear cells in postmenopausal osteoporosis. FASEB J 19: 410-2

D'Amelio P, Sassi F, Buondonno I, Fornelli G, Spertino E, D'Amico L, Marchetti M, Lucchiari M, Roato I, Isaia GC (2015) Treatment with intermittent PTH increases Wnt10b production by T cells in osteoporotic patients. Osteoporos Int 26: 2785-91
Dempster DW, Compston JE, Drezner MK, Glorieux FH, Kanis JA, Malluche H, Meunier PJ, Ott SM, Recker RR, Parfitt AM (2013) Standardized nomenclature, symbols, and units for bone histomorphometry: a 2012 update of the report of the ASBMR Histomorphometry Nomenclature Committee. J Bone Miner Res 28: 2-17
Di Ianni M, Falzetti F, Carotti A, Terenzi A, Castellino F, Bonifacio E, Del Papa B, Zei T, Ostini RI, Cecchini D, Aloisi T, Perruccio K, Ruggeri L, Balucani C, Pierini A, Sportoletti P, Aristei C, Falini B, Reisner Y, Velardi A et al. (2011) Tregs prevent GVHD and promote immune reconstitution in HLA-haploidentical transplantation. Blood 117: 3921-8
Dichlberger A, Schlager S, Maaninka K, Schneider WJ, Kovanen PT (2014) Adipose triglyceride lipase regulates eicosanoid production in activated human mast cells. J Lipid Res 55: 2471-8
Duarte JH, Zelenay S, Bergman ML, Martins AC, Demengeot J (2009) Natural Treg cells spontaneously differentiate into pathogenic helper cells in lymphopenic conditions. European journal of immunology 39: 948-55
Esen E, Lee SY, Wice BM, Long F (2015) PTH Promotes Bone Anabolism by Stimulating Aerobic Glycolysis via IGF Signaling. J Bone Miner Res 30: 1959-68
Fantini MC, Dominitzki S, Rizzo A, Neurath MF, Becker C (2007) In vitro generation of CD4+ CD25+ regulatory cells from murine naive T cells. Nature protocols 2: 1789-94
Fehr T, Lucas CL, Kurtz J, Onoe T, Zhao G, Hogan T, Vallot C, Rao A, Sykes M (2010) A CD8 T cell-intrinsic role for the calcineurin-NFAT pathway for tolerance induction in vivo. Blood 115: 1280-7
Feng F, Hu P, Chen L, Tang Q, Lian C, Yao Q, Chen K (2013) Display of human proinsulin on the Bacillus subtilis spore surface for oral administration. Current microbiology 67: 1-8
Grey AB, Stapleton JP, Evans MC, Reid IR (1996) Accelerated bone loss in post-menopausal women with mild primary hyperparathyroidism. Clin Endocrinol (Oxf) 44: 697-702
Guo J, Liu M, Yang D, Bouxsein ML, Saito H, Galvin RJ, Kuhstoss SA, Thomas CC, Schipani E, Baron R, Bringhurst FR, Kronenberg HM (2010) Suppression of Wnt signaling by Dkk1 attenuates PTH-mediated stromal cell response and new bone formation. Cell metabolism 11: 161-71
Heissmeyer V, Macian F, Im SH, Varma R, Feske S, Venuprasad K, Gu H, Liu YC, Dustin ML, Rao A (2004) Calcineurin imposes T cell unresponsiveness through targeted proteolysis of signaling proteins. Nat Immunol 5: 255-65
Huang H, Chikazu D, Voznesensky OS, Herschman HR, Kream BE, Drissi H, Pilbeam CC (2010) Parathyroid hormone induction of cyclooxygenase-2 in murine osteoblasts: role of the calcium-calcineurin-NFAT pathway. J Bone Miner Res 25: 819-29
Jilka RL (2007) Molecular and cellular mechanisms of the anabolic effect of intermittent PTH. Bone 40: 1434-46
Johannesson B, Sattler S, Semenova E, Pastore S, Kennedy-Lydon TM, Sampson RD, Schneider MD, Rosenthal N, Bilbao D (2014) Insulin-like growth factor-1 induces regulatory T cell-mediated suppression of allergic contact dermatitis in mice. Dis Model Mech 7: 977-85
Karlsson F, Robinson-Jackson SA, Gray L, Zhang S, Grisham MB (2011) Ex vivo generation of regulatory T cells: characterization and therapeutic evaluation in a model of chronic colitis. Methods Mol Biol 677: 47-61
Kelchtermans H, Geboes L, Mitera T, Huskens D, Leclercq G, Matthys P (2009) Activated CD4+CD25+ regulatory T cells inhibit osteoclastogenesis and collagen-induced arthritis. Ann Rheum Dis 68: 744-50
Keller H, Kneissel M (2005) SOST is a target gene for PTH in bone. Bone 37: 148-58

Kim YG, Lee CK, Nah SS, Mun SH, Yoo B, Moon HB (2007) Human CD4+CD25+ regulatory T cells inhibit the differentiation of osteoclasts from peripheral blood mononuclear cells. Biochem Biophys Res Commun 357: 1046-52
Klingenberg R, Gerdes N, Badeau RM, Gistera A, Strodthoff D, Ketelhuth DF, Lundberg AM, Rudling M, Nilsson SK, Olivecrona G, Zoller S, Lohmann C, Luscher TF, Jauhiainen M, Sparwasser T, Hansson GK (2013) Depletion of FOXP3+ regulatory T cells promotes hypercholesterolemia and atherosclerosis. J Clin Invest 123: 1323-34
Koh AJ, Novince CM, Li X, Wang T, Taichman RS, McCauley LK (2011) An irradiation-altered bone marrow microenvironment impacts anabolic actions of PTH. Endocrinology 152: 4525-36
Kramer I, Loots GG, Studer A, Keller H, Kneissel M (2010) Parathyroid hormone (PTH)-induced bone gain is blunted in SOST overexpressing and deficient mice. J Bone Miner Res 25: 178-89
Lahl K, Loddenkemper C, Drouin C, Freyer J, Arnason J, Eberl G, Hamann A, Wagner H, Huehn J, Sparwasser T (2007) Selective depletion of Foxp3+ regulatory T cells induces a scurfy-like disease. J Exp Med 204: 57-63
Lahl K, Sparwasser T (2011) In vivo depletion of FoxP3+ Tregs using the DEREG mouse model. Methods Mol Biol 707: 157-72
Lanske B, Amling M, Neff L, Guiducci J, Baron R, Kronenberg HM (1999) Ablation of the PTHrP gene or the PTH/PTHrP receptor gene leads to distinct abnormalities in bone development. J Clin Invest 104: 399-407
Li JY, Adams J, Calvi LM, Lane TF, DiPaolo R, Weitzmann MN, Pacifici R (2012) PTH expands short-term murine hemopoietic stem cells through T cells. Blood 120: 4352-62
Li JY, Chassaing B, Tyagi AM, Vaccaro C, Luo T, Adams J, Darby TM, Weitzmann MN, Mulle JG, Gewirtz AT, Jones RM, Pacifici R (2016) Sex steroid deficiency-associated bone loss is microbiota dependent and prevented by probiotics. J Clin Invest
Li JY, D'Amelio P, Robinson J, Walker LD, Vaccaro C, Luo T, Tyagi AM, Yu M, Reott M, Sassi F, Buondonno I, Adams J, Weitzmann MN, Isaia GC, Pacifici R (2015) IL-17A Is Increased in Humans with Primary Hyperparathyroidism and Mediates PTH-Induced Bone Loss in Mice. Cell metabolism 22: 799-810
Li JY, Walker LD, Tyagi AM, Adams J, Weitzmann MN, Pacifici R (2014) The sclerostin-independent bone anabolic activity of intermittent PTH treatment is mediated by T-cell-produced Wnt10b. J Bone Miner Res 29: 43-54
Liu Y, Zhang P, Li J, Kulkarni AB, Perruche S, Chen W (2008) A critical function for TGF-beta signaling in the development of natural CD4+CD25+Foxp3+ regulatory T cells. Nat Immunol 9: 632-40
Macian F (2005) NFAT proteins: key regulators of T-cell development and function. Nature reviews 5: 472-84
Macian F, Garcia-Cozar F, Im SH, Horton HF, Byrne MC, Rao A (2002) Transcriptional mechanisms underlying lymphocyte tolerance. Cell 109: 719-31
Marek-Trzonkowska N, Mysliwiec M, Dobyszuk A, Grabowska M, Techmanska I, Juscinska J, Wujtewicz MA, Witkowski P, Mlynarski W, Balcerska A, Mysliwska J, Trzonkowski P (2012) Administration of CD4+CD25highCD127- regulatory T cells preserves beta-cell function in type 1 diabetes in children. Diabetes care 35: 1817-20
McCarthy TL, Centrella M, Canalis E (1989) Parathyroid hormone enhances the transcript and polypeptide levels of insulin-like growth factor I in osteoblast-enriched cultures from fetal rat bone. Endocrinology 124: 1247-53
Najafian N, Sayegh MH (2000) CTLA4-Ig: a novel immunosuppressive agent. Expert opinion on investigational drugs 9: 2147-57
Ohkura N, Kitagawa Y, Sakaguchi S (2013) Development and maintenance of regulatory T cells. Immunity 38: 414-23

Oursler MJ, Cortese C, Keeting P, Anderson MA, Bonde SK, Riggs BL, Spelsberg TC (1991) Modulation of transforming growth factor-beta production in normal human osteoblast-like cells by 17 beta-estradiol and parathyroid hormone. Endocrinology 129: 3313-3320
Pacifici R (2013) Role of T cells in the modulation of PTH action: physiological and clinical significance. Endocrine 44: 576-82
Park HJ, Baek K, Baek JH, Kim HR (2015) The cooperation of CREB and NFAT is required for PTHrP-induced RANKL expression in mouse osteoblastic cells. J Cell Physiol 230: 667-79
Pfeilschifter J, Laukhuf F, Muller-Beckmann B, Blum WF, Pfister T, Ziegler R (1995) Parathyroid hormone increases the concentration of insulin-like growth factor-I and transforming growth factor beta 1 in rat bone. J Clin Invest 96: 767-74
Potts J (1998) Primary hyperparathyroidism. In Metabolic Bone Diseases, Avioli LV, Krane S (eds) pp 411-442. San Diego: Academic Press
Powell WF, Jr., Barry KJ, Tulum I, Kobayashi T, Harris SE, Bringhurst FR, Pajevic PD (2011) Targeted ablation of the PTH/PTHrP receptor in osteocytes impairs bone structure and homeostatic calcemic responses. J Endocrinol 209: 21-32
Qin L, Raggatt LJ, Partridge NC (2004) Parathyroid hormone: a double-edged sword for bone metabolism. Trends Endocrinol Metab 15: 60-5
Rhee Y, Allen MR, Condon K, Lezcano V, Ronda AC, Galli C, Olivos N, Passeri G, O'Brien CA, Bivi N, Plotkin LI, Bellido T (2011) PTH receptor signaling in osteocytes governs periosteal bone formation and intracortical remodeling. J Bone Miner Res 26: 1035-46
Robinson JW, Li JY, Walker LD, Tyagi AM, Reott MA, Yu M, Adams J, Weitzmann MN, Pacifici R (2015) T cell-expressed CD40L potentiates the bone anabolic activity of intermittent PTH treatment. J Bone Miner Res 30: 695-705
Roncador G, Brown PJ, Maestre L, Hue S, Martinez-Torrecuadrada JL, Ling KL, Pratap S, Toms C, Fox BC, Cerundolo V, Powrie F, Banham AH (2005) Analysis of FOXP3 protein expression in human CD4+CD25+ regulatory T cells at the single-cell level. European journal of immunology 35: 1681-91
Roser-Page S, Vikulina T, Zayzafoon M, Weitzmann MN (2014) CTLA-4Ig-induced T cell anergy promotes Wnt-10b production and bone formation in a mouse model. Arthritis & rheumatology 66: 990-9
Saini V, Marengi DA, Barry KJ, Fulzele KS, Heiden E, Liu X, Dedic C, Maeda A, Lotinun S, Baron R, Pajevic PD (2013) Parathyroid hormone (PTH)/PTH-related peptide type 1 receptor (PPR) signaling in osteocytes regulates anabolic and catabolic skeletal responses to PTH. The Journal of biological chemistry 288: 20122-34
Schmidt A, Oberle N, Krammer PH (2012) Molecular mechanisms of treg-mediated T cell suppression. Front Immunol 3: 51
Setiady YY, Coccia JA, Park PU (2010) In vivo depletion of CD4+FOXP3+ Treg cells by the PC61 anti-CD25 monoclonal antibody is mediated by FcgammaRIII+ phagocytes. European journal of immunology 40: 780-6
Shevach EM (2009) Mechanisms of foxp3+ T regulatory cell-mediated suppression. Immunity 30: 636-45
Silvestrini G, Ballanti P, Leopizzi M, Sebastiani M, Berni S, Di Vito M, Bonucci E (2007) Effects of intermittent parathyroid hormone (PTH) administration on SOST mRNA and protein in rat bone. J Mol Histol 38: 261-9
Tan C, Reddy V, Dannull J, Ding E, Nair SK, Tyler DS, Pruitt SK, Lee WT (2013) Impact of anti-CD25 monoclonal antibody on dendritic cell-tumor fusion vaccine efficacy in a murine melanoma model. Journal of translational medicine 11: 148
Terauchi M, Li JY, Bedi B, Baek KH, Tawfeek H, Galley S, Gilbert L, Nanes MS, Zayzafoon M, Guldberg R, Lamar DL, Singer MA, Lane TF, Kronenberg HM, Weitzmann MN, Pacifici R (2009) T lymphocytes amplify the anabolic activity of parathyroid hormone through Wnt10b signaling. Cell metabolism 10: 229-40

Tone Y, Furuuchi K, Kojima Y, Tykocinski ML, Greene MI, Tone M (2008) Smad3 and NFAT cooperate to induce Foxp3 expression through its enhancer. Nat Immunol 9: 194-202
Trzonkowski P, Bieniaszewska M, Juscinska J, Dobyszuk A, Krzystyniak A, Marek N, Mysliwska J, Hellmann A (2009) First-in-man clinical results of the treatment of patients with graft versus host disease with human ex vivo expanded CD4+CD25+CD127- T regulatory cells. Clin Immunol 133: 22-6
Uzawa T, Hori M, Ejiri S, Ozawa H (1995) Comparison of the effects of intermittent and continuous administration of human parathyroid hormone(1-34) on rat bone. Bone 16: 477-84
von Boehmer H, Daniel C (2013) Therapeutic opportunities for manipulating T(Reg) cells in autoimmunity and cancer. Nat Rev Drug Discov 12: 51-63
Wan M, Yang C, Li J, Wu X, Yuan H, Ma H, He X, Nie S, Chang C, Cao X (2008) Parathyroid hormone signaling through low-density lipoprotein-related protein 6. Genes Dev 22: 2968-79
Wing K, Onishi Y, Prieto-Martin P, Yamaguchi T, Miyara M, Fehervari Z, Nomura T, Sakaguchi S (2008) CTLA-4 control over Foxp3+ regulatory T cell function. Science 322: 271-5
Wu Y, Kumar R (2000) Parathyroid hormone regulates transforming growth factor beta1 and beta2 synthesis in osteoblasts via divergent signaling pathways. J Bone Miner Res 15: 879-84
Yuan FL, Li X, Lu WG, Xu RS, Zhao YQ, Li CW, Li JP, Chen FH (2010) Regulatory T cells as a potent target for controlling bone loss. Biochemical and biophysical research communications 402: 173-6
Zaidi M (2007) Skeletal remodeling in health and disease. Nat Med 13: 791-801
Zaiss MM, Axmann R, Zwerina J, Polzer K, Guckel E, Skapenko A, Schulze-Koops H, Horwood N, Cope A, Schett G (2007) Treg cells suppress osteoclast formation: a new link between the immune system and bone. Arthritis Rheum 56: 4104-12
Zaiss MM, Sarter K, Hess A, Engelke K, Bohm C, Nimmerjahn F, Voll R, Schett G, David JP (2010) Increased bone density and resistance to ovariectomy-induced bone loss in FoxP3-transgenic mice based on impaired osteoclast differentiation. Arthritis and rheumatism 62: 2328-38

Table 1. Demographic and clinical data of patients with postmenopausal osteoporosis treated with calcium and vitamin D, or calcium and vitamin D and Teriparatide. Data are shown as Mean ± SEM, p values were calculated by unpaired t-test. Values in squared parenthesis denote normal range.

	Control	Teriparatide	p
n	20	20	
Age	68.5 ± 1.8	69.7 ± 1.6	0.535
Years since menopause	18.4 ± 2.1	20.8 ± 1.6	0.232
Ca (mg/dL) [8.8-10.4 mg/dl]	9.6 ± 0.1	9.5 ± 0.1	0.851
Serum P (mg/dL) [2.5-4.48 mg/dl]	3.5 ± 0.2	3.4 ± 0.1	0.608
PTH (pg/mL) [10-65 pg/mL]	42.8 ± 9.3	46.8 ± 4.1	0.272
25OH vitamin D (ng/mL) [20-100 ng/mL]	30.2 ± 3.1	27.3 ± 2.7	0.997

FIGURE LEGEND

Figure 1. Teriparatide treatment in humans increases the absolute and relative number of Tregs in peripheral blood and TGF expression by Tregs. **A.** Relative frequency of Tregs in PBMC at 3 and 6 months of treatment. n = 17 patients per group. **B.** Absolute frequency of Tregs in PBMC at 3 and 6 months of treatment. n = 20 patients per group. **C.** mRNA levels of TGFβ1 in peripheral blood CD4+CD25+ T cells at 3 and 6 months of treatment. n = 9 patients per group. **D.** Relative frequency of Tregs in cultures of in peripheral blood CD4+CD25+ T cells stimulated with vehicle or PTH. **E.** mRNA levels of TGFβ1 in peripheral blood CD4+CD25+ T cells stimulated with vehicle or PTH. All data are expressed as Mean ± SEM. All data were normally distributed according to the Shapiro-Wilk normality test and analyzed by 2-way ANOVA for repeated measures. *= $p<0.05$, **= $p<0.01$, and ***= $p<0.001$ compared to baseline. # = $p<0.05$, and ## = $p<0.01$, compared to Ca + D group.

Figure 2. iPTH treatment increases the number of BM Tregs and Treg differentiation. To determine the effect of treatment on the number of Tregs, BM TCRβ+CD4+Foxp3+ T cells were counted by flow cytometry following 1, 2 and 4 weeks of treatment with vehicle or iPTH. To assess Treg differentiation, conventional CD4+ T cells (TCRβ+CD4+eGFP-) from B6.Foxp3.eGFP reporter mice were transferred into TCRβ-/-mice. Recipient mice were treated with vehicle or iPTH for 1,2 or 4 weeks starting 2 weeks after the T cell transfer. The number of BM TCRβ+CD4+eGFP+ cells was then determined by flow cytometry. **A.** Relative frequency of BM Tregs at 1, 2 and 4 weeks of treatment. n = 10-32 mice per group. **B.** Absolute frequency of Tregs at 1, 2, and 4 weeks of treatment. n = 10-32 mice per group. **C.** Relative frequency of eGFP+ Tregs at 1, 2, and 4 weeks of treatment n = 10 mice per group. **D.** Absolute frequency of eGFP+ Tregs at 1, 2, and 4 weeks of treatment n = 10 mice per group. Data are expressed as

Mean ± SEM. All data were normally distributed according to the Shapiro-Wilk normality test and analyzed by unpaired T tests. ***= p<0.001, and ****= p<0.0001 compared to the corresponding vehicle.

Figure 3. Depletion of Tregs by treatment with anti-CD25 Ab prevents the bone anabolic activity of iPTH. **A,B.** Relative and absolute frequency of BM Tregs. **C**. Wnt10b mRNA levels in BM CD8+ T cells. **D.** Images of representative 3-dimensional μCT reconstructions of examined femurs from each group **E.** Femoral trabecular bone volume (BV/TV) as measured by μCT scanning. **F.** Femoral cortical bone volume (Ct.Vo) by μCT scanning **G**. Images are representative sections displaying the calcein double-fluorescence labeling. Original magnification x 20. **H**. Mineral apposition rate (MAR), **I**. Bone formation rate per mm bone surface (BFR/BS). **J.** The number of osteoblasts per mm bone surface (N.Ob/BS). **K**. The percentage of bone surface covered by osteoblasts (Ob.S/BS). **L**. The images show tartrate resistant acid phosphatase (TRAP) stained sections of the distal femur. Original magnification x 40. **M**. The number of osteoclasts per mm bone surface (N.Oc/BS). **N**. The percentage of bone surface covered by osteoclasts (Oc.S/BS). **O.** Serum levels of osteocalcin (OCN), a marker of bone formation. **P.** Serum levels of type 1 cross-linked C-telopeptide (CTX), a marker of resorption. n=10-25 mice per group. Data are expressed as Mean ± SEM. All data were normally distributed according to the Shapiro-Wilk normality test and analyzed by two-way analysis-of-variance and post hoc tests applying the Bonferroni correction for multiple comparisons. *=p<0.05, **=p<0.01, ***=p<0.001 and ****= p<0.0001 compared to the indicated group.

Figure 4. Depletion of Tregs by treatment of DEREG mice with diphtheria toxin (DT) prevents the bone anabolic activity of iPTH. **A,B**. Relative and absolute frequency of BM Tregs. **C.** Wnt10b mRNA levels in BM CD8+ T cells. **D.** Images of representative 3-dimensional μCT reconstructions of examined femurs from each group. **E**. Femoral trabecular bone volume

(BV/TV) as measured by μCT scanning. **F.** Femoral cortical bone volume (Ct.Vo) by μCT scanning. **G**. Images are representative sections displaying the calcein double-fluorescence labeling. Original magnification x 20. **H**. Mineral apposition rate (MAR). **I**. Bone formation rate (BFR). **J** The number of osteoblasts per mm bone surface (N.Ob/BS). **K**. The percentage of bone surface covered by osteoblasts (Ob.S/BS). **L**. The images show tartrate resistant acid phosphatase (TRAP) stained sections of the distal femur. Original magnification x 40. **M**. The number of osteoclasts per mm bone surface (N.Oc/BS). **N**. The percentage of bone surface covered by osteoclasts (Oc.S/BS). **O.** Serum levels of osteocalcin, a marker of bone formation. **P**. Serum levels of type 1 cross-linked C-telopeptide (CTX), a marker of resorption. n=9-13 mice per group. Data are expressed as Mean ± SEM. All data were normally distributed according to the Shapiro-Wilk normality test and analyzed by two-way analysis-of-variance and post hoc tests applying the Bonferroni correction for multiple comparisons. *=$p<0.05$, **=$p<0.01$, ***=$p<0.001$ and ****= $p<0.0001$ compared to the indicated group.

Figure 5. iPTH increases Wnt10b transcription by promoting the binding of NFAT/SMAD complexes to the Wnt10b promoter. A. Expression of Wnt10b mRNA by sorted BM conventional CD4+ cells (TCRβ+CD4+eGFP- cells), Tregs (TCRβ+CD4+ eGFP + cells) and CD8+ T cells from B6.Foxp3.eGFP reporter mice treated with vehicle or iPTH for 4 weeks. **B**. The NFAT activator ionomycin and TGFβ stimulate Wnt10b mRNA expression in splenic CD8+ T cells. **C**. ChIP assays demonstrating that in vivo iPTH treatment increases the binding of NFAT1, NFAT2 and SMAD3, but not of SMAD2, to the Wnt10b promoter in BM CD8+ T cells. Cells from 4-5 mice were pooled to generate 1 sample. **D**. Diagrammatic representation of the Wnt10b promoter and effects of promoter deletion on the activity of Wnt10b-luciferase reporter constructs in primary splenic CD8+ T cells and EL4 T cells. Cells were stimulated with Ionomycin (500 ng/ml) and TGFβ (5 ng/ml) for 24 hours to induce reporter activity. n= 3 samples per group. **E**. Effects of mutation of the SMAD and NFAT binding sites on the Wnt10b promoter

on the activity of a luciferase-Wnt10b reporter constructs in primary splenic CD8+ T cells and EL4 cells. Cells were stimulated with Ionomycin (500 ng/ml) and TGFβ (5 ng/ml) for 24 hours to induce reporter activity. Data are expressed as Mean ± SEM. Data were analyzed by Kruskal-Wallis and Dunn's multiple comparisons non-parametric tests, as they were not normally distributed as assessed by Shapiro-Wilk normality test. Panel A: n = 5 per group, ****= p<0.0001 compared the corresponding vehicle group; Panel B: n = 3 per group, * = p <0.05, and ****= p<0.0001 compared the corresponding time 0. Panels C-E: n= 3 samples per group, , **= p<0.01, ***= p<0.001 and ****= p<0.0001 compared to Veh Irr.Ab or empty vector.

Figure 6. Effects of PTH and Tregs on NFAT1/2 and SMAD2/3 activation in CD8+ T cells. **A.** Western blotting analysis of NFAT1, NFAT2, pSMAD2, and pSMAD3 in BM CD8+ T cells. The figure shows one representative experiment of 3 experiments. **B,C.** Relative and absolute frequency of BM LAP+ Tregs. **D.** TGFβ1 protein levels in purified BM CD4+ T cells culture media. **E.** mRNA levels of TGFβ1 in BM Tregs. **F**. TGFβ1 mRNA expression by purified BM cells populations. **G**. Western blotting analysis of NFAT1, NFAT2, pSMAD2, pSMAD3, c-Jun and c-Fos in purified splenic CD8+ T cells. CD8+ T cells were unstimulated, activated with OVA peptide pulsed DCs with and without induced Tregs for 2h. The figure shows one representative experiment of 3 experiments. **H**. Western blotting analysis of c-Fos and c-Jun in BM CD8+ T cells. The figure shows one representative experiment of 3 experiments. R.I.= Relative Intensity. **I**. Coculture with induced Tregs increases the baseline and the PTH-induced expression of Wnt10b by CD8+ T cells in an APC assay. **J**. Western blotting analysis of NFAT1, NFAT2, pSMAD2, pSMAD3, c-Jun and c-Fos in purified splenic CD8+ T cells stimulated with PTH (100 nM for 30 min). CD8+ T cells were unstimulated, activated with OVA peptide pulsed DCs with and without CD28 signaling blocking by CTLA-4-Ig treatment. The figure shows one representative experiment of 3 experiments. In panels A,F,G,I, Laminin B1 was used as nuclear loading control. Tubulin was used as cytoplasmic loading control. **K**. Blockade of CD28

signaling by CTLA-4-Ig increases the baseline and the PTH-induced expression of Wnt10b by CD8+ T cells in an APC assay. **L**. Activation of TCR signaling in the absence of CD28 signaling stimulates Wnt10b gene expression in primary splenic CD8+ T cells. The NFAT inhibitor 11R VIVIT blocks Wnt10b gene expression in the absence of CD28 stimulation. Panels B-F and I,K: n = 5-8 mice per group. Data are expressed as mean ± SEM. Panels B-F and I,K: Data were analyzed by unpaired t-tests or two-way analysis-of-variance and post hoc tests applying the Bonferroni correction for multiple comparisons. Panel L: Data were analyzed by Kruskal-Wallis non-parametric test as they were not normally distributed as assessed by Shapiro-Wilk normality test. * = $p < 0.05$, **= $p < 0.01$, ***= $p < 0.001$ and ****= $p < 0.0001$ compared to vehicle or the indicated group.

Figure 7. Effects of iPTH treatment on CD28 signaling in BM T cells and the expression of CD80 and CD86 on BM mature dendritic cells (DCs). **A**. Western blotting analysis of Phospho-PI3K p85 in BM CD8+ T cells. The figure shows one representative experiment of 5 total experiments. R.I.= Relative Intensity. **B**. % of pAKT+ BM CD8+ T cells. **C**. pAKT levels in BM C8+ T cells. **D**. Relative frequency of BM CD80+ mature DCs. **E**. Absolute frequency of BM CD80+ mature DCs. **F**. Relative frequency of BM CD86+ mature DCs. **G**. Absolute frequency of BM CD86+ mature DCs. Panels B,C: n = 5-8 mice per group. Panels D-G: n = 12 mice per group. Data are expressed as mean + SEM. Data were analyzed by unpaired t-tests or two-way analysis-of-variance and post hoc tests applying the Bonferroni correction for multiple comparisons. **= $p < 0.01$, ***= $p < 0.001$ and ****= $p < 0.0001$ compared to vehicle or the indicated group.

Figure 8. Diagrammatic representation of the mechanism by which iPTH treatment stimulates bone formation and increases bone mass. iPTH increases the differentiation of naïve CD4+ T cells into Tregs and expands the pool of BM Tregs by up-regulating the production of IGF-1 and TGF in BM microenvironment and by increasing the sensitivity of conventional CD4+ T cells to TGF. mature Tregs do not express PPR and are not directly targeted by iPTH. Membrane-

bound TGF produced by Tregs activates SMAD signaling in CD8+ T cells while iPTH activates NFAT signaling in CD8+ T cells. Moreover, Tregs downregulate CD28 signaling in CD8+ T cells, lowering the activation of AP-1, thus preventing the association of NFAT and AP-1. In such conditions of low AP-1 levels, NFAT bind together with SMAD to the Wnt10 promoter activating Wnt10b transcription. Direct stimulation of CD8+ T cells by iPTH further upregulate Wnt10b gene expression. Wnt10b is known to activate Wnt signaling in mesenchymal stem cells and their osteogenic progeny, leading to increased osteoblast proliferation and differentiation and lower osteoblast apoptosis. This increase in osteoblastogenesis and osteoblast life span increases bone formation and bone trabecular bone volume.

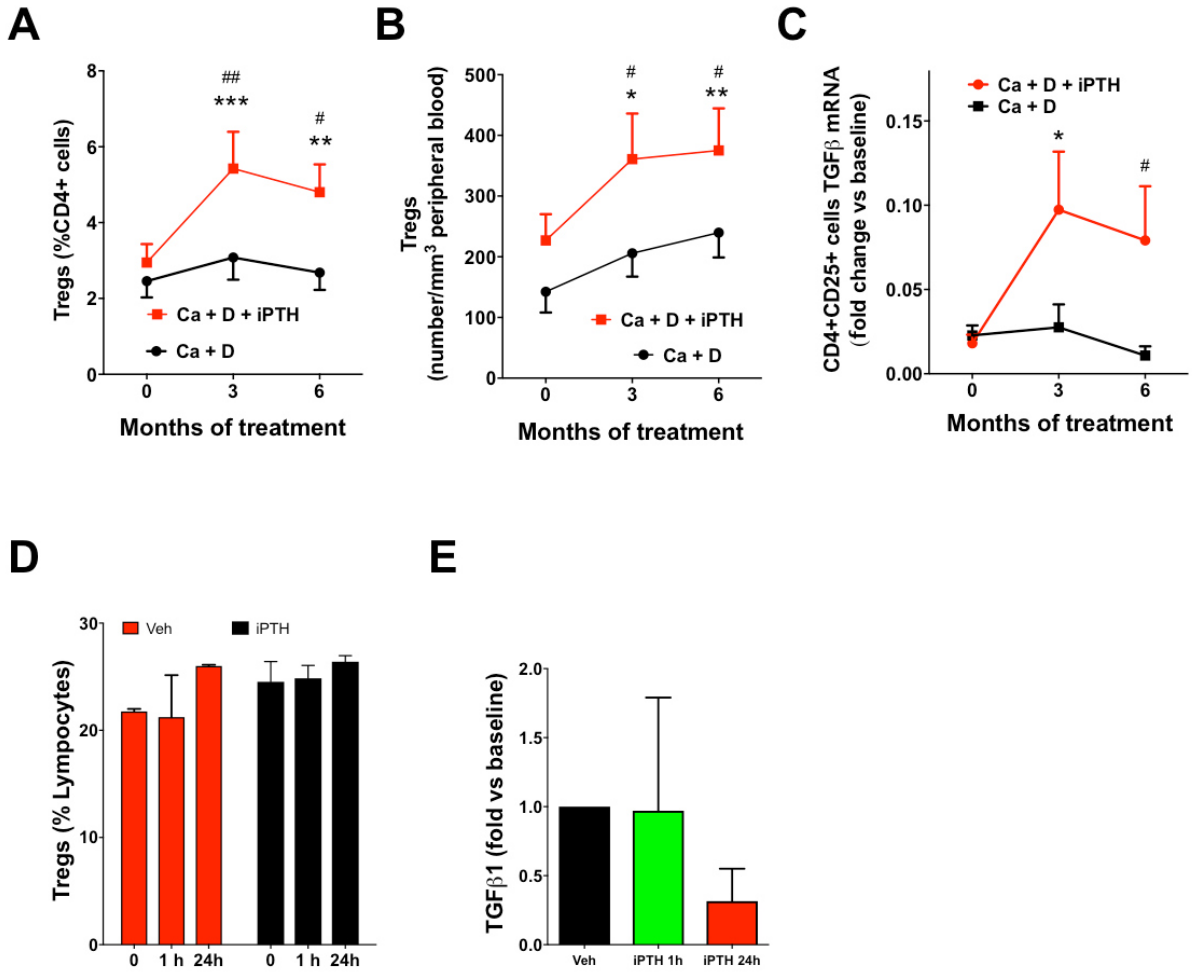

Figure 1. Teriparatide treatment in humans increases the absolute and relative number of Tregs in peripheral blood and TGFβ expression by Tregs. **A.** Relative frequency of Tregs in PBMC at 3 and 6 months of treatment. n = 17 patients per group. **B.** Absolute frequency of Tregs in PBMC at 3 and 6 months of treatment. n = 20 patients per group. **C.** mRNA levels of TGFβ1 in peripheral blood CD4+CD25+ T cells at 3 and 6 months of treatment. n = 9 patients per group. **D.** Relative frequency of Tregs in cultures of in peripheral blood CD4+CD25+ T cells stimulated with vehicle or PTH. **E.** mRNA levels of TGFβ1 in peripheral blood CD4+CD25+ T cells stimulated with vehicle or PTH. All data are expressed as Mean ± SEM. All data were normally distributed according to the Shapiro-Wilk normality test and analyzed by 2-way ANOVA for repeated measures. *= $p<0.05$, **= $p<0.01$, and ***= $p<0.001$ compared to baseline. # = $p<0.05$, and ## = $p<0.01$, compared to Ca + D group.

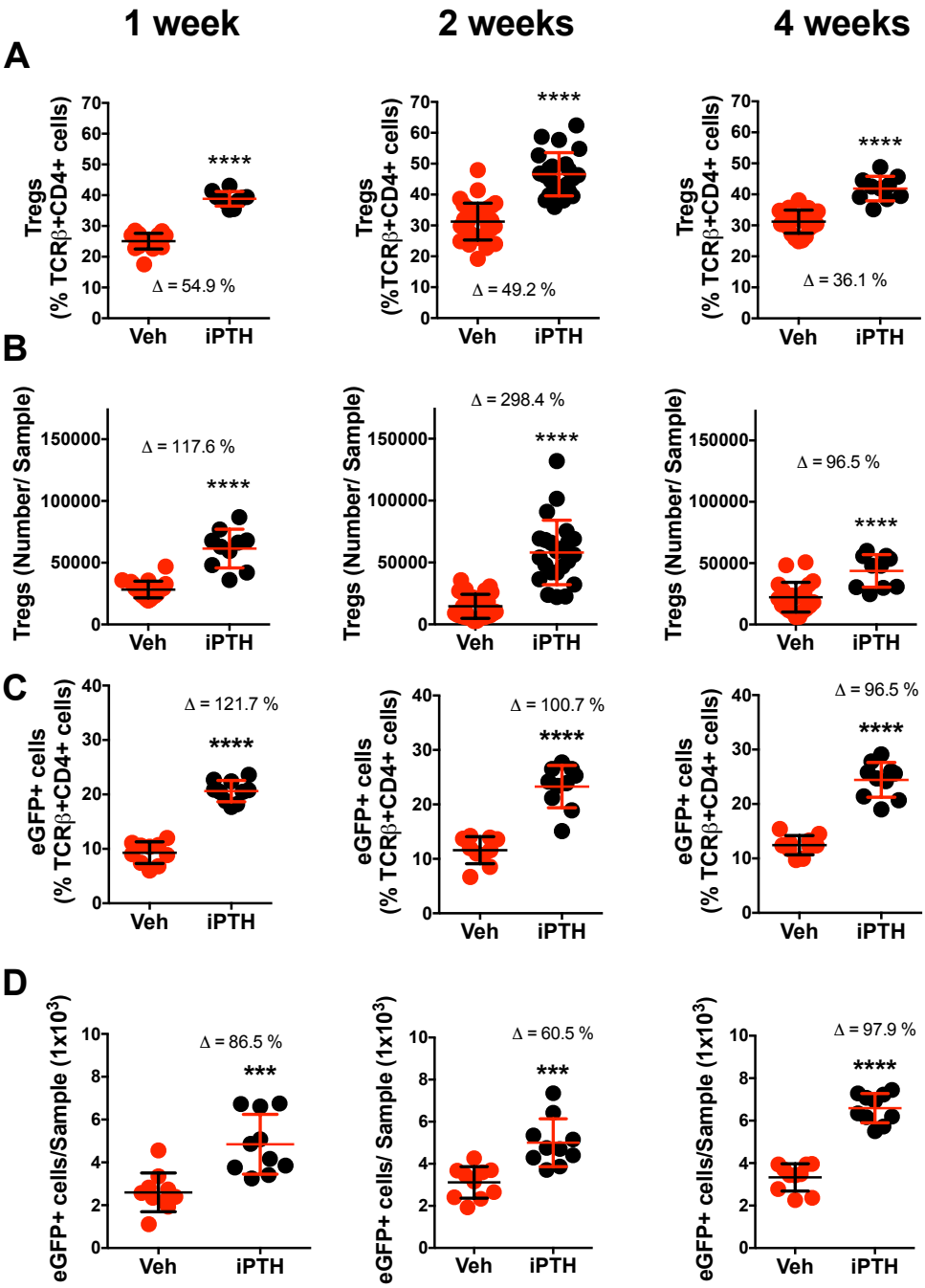

Figure 2. iPTH treatment increases the number of BM Tregs and Treg differentiation. To determine the effect of treatment on the number of Tregs, BM TCRβ+CD4+Foxp3+ T cells were counted by flow cytometry following 1, 2 and 4 weeks of treatment with vehicle or iPTH. To assess Treg differentiation, conventional CD4+ T cells (TCRβ+CD4+eGFP-) from B6.Foxp3.eGFP reporter mice were transferred into TCRβ-/-mice. Recipient mice were treated with vehicle or iPTH for 1,2 or 4 weeks starting 2 weeks after the T cell transfer. The number of BM TCRβ+CD4+eGFP+ cells was then determined by flow cytometry. **A.** Relative frequency of BM Tregs at 1, 2 and 4 weeks of treatment. n = 10-32 mice per group. **B.** Absolute frequency of Tregs at 1, 2, and 4 weeks of treatment. n = 10-32 mice per group. **C.** Relative frequency of eGFP+ Tregs at 1, 2, and 4 weeks of treatment n = 10 mice per group. **D.** Absolute frequency of eGFP+ Tregs at 1, 2, and 4 weeks of treatment n = 10 mice per group. Data are expressed as Mean ± SEM. All data were normally distributed according to the Shapiro-Wilk normality test and analyzed by unpaired T tests. ***= $p<0.001$, and ****= $p<0.0001$ compared to the corresponding vehicle.

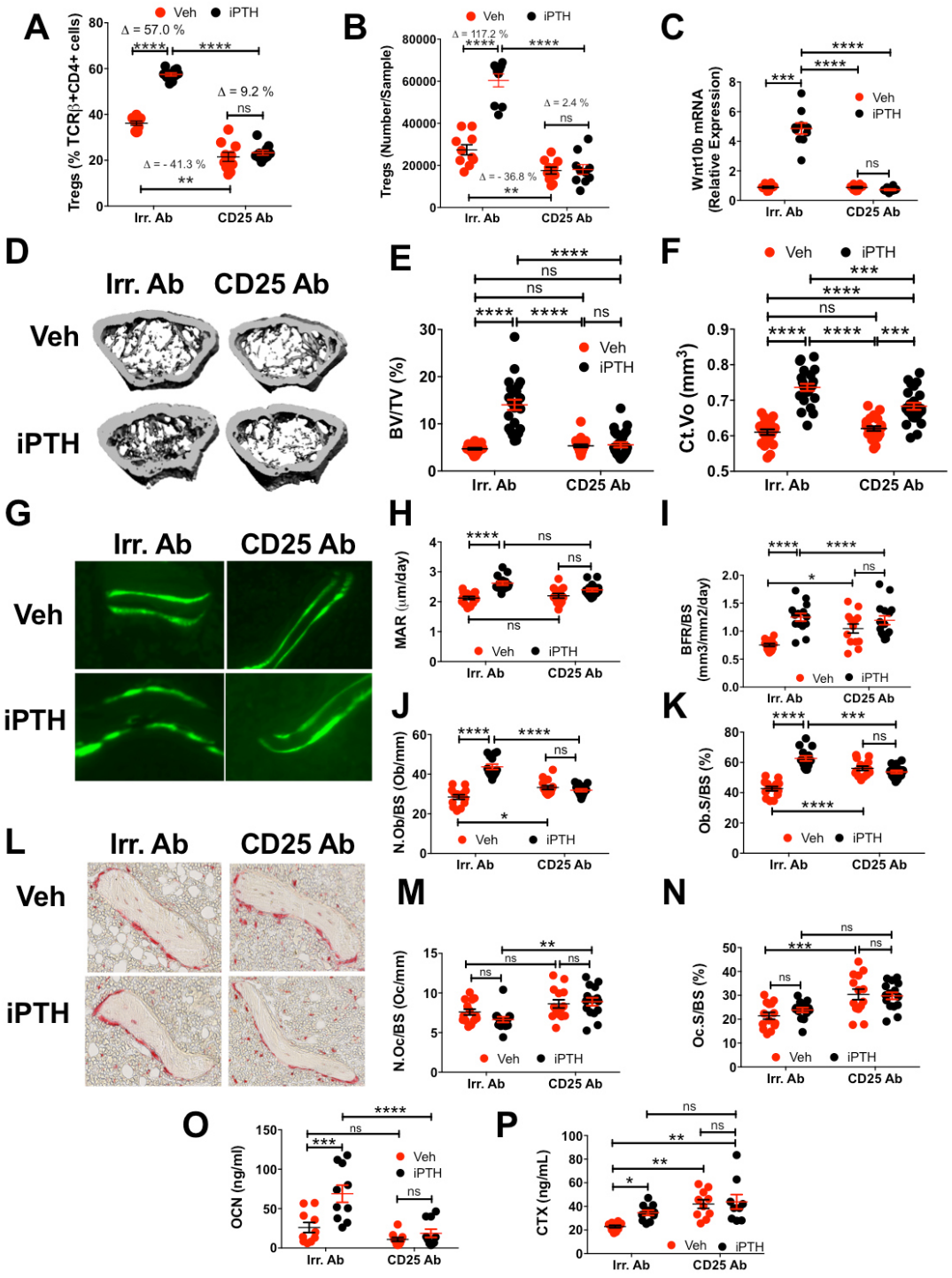

Figure 3. Depletion of Tregs by treatment with anti-CD25 Ab prevents the bone anabolic activity of iPTH. **A,B.** Relative and absolute frequency of BM Tregs. **C**. Wnt10b mRNA levels in BM CD8+ T cells. **D.** Images of representative 3-dimensional μCT reconstructions of examined femurs from each group **E.** Femoral trabecular bone volume (BV/TV) as measured by μCT scanning. **F.** Femoral cortical bone volume (Ct.Vo) by μCT scanning **G**. Images are representative sections displaying the calcein double-fluorescence labeling. Original magnification x 20. **H**. Mineral apposition rate (MAR), **I**. Bone formation rate per mm bone surface (BFR/BS). **J.** The number of osteoblasts per mm bone surface (N.Ob/BS). **K**. The percentage of bone surface covered by osteoblasts (Ob.S/BS). **L**. The images show tartrate resistant acid phosphatase (TRAP) stained sections of the distal femur. Original magnification x 40. **M**. The number of osteoclasts per mm bone surface (N.Oc/BS). **N**. The percentage of bone surface covered by osteoclasts (Oc.S/BS). **O.** Serum levels of osteocalcin (OCN), a marker of bone formation. **P.** Serum levels of type 1 cross-linked C-telopeptide (CTX), a marker of resorption. n=10-25 mice per group. Data are expressed as Mean ± SEM. All data were normally distributed according to the Shapiro-Wilk normality test and analyzed by two-way analysis-of-variance and post hoc tests applying the Bonferroni correction for multiple comparisons. *=p<0.05, **=p<0.01, ***=p<0.001 and ****= p<0.0001 compared to the indicated group.

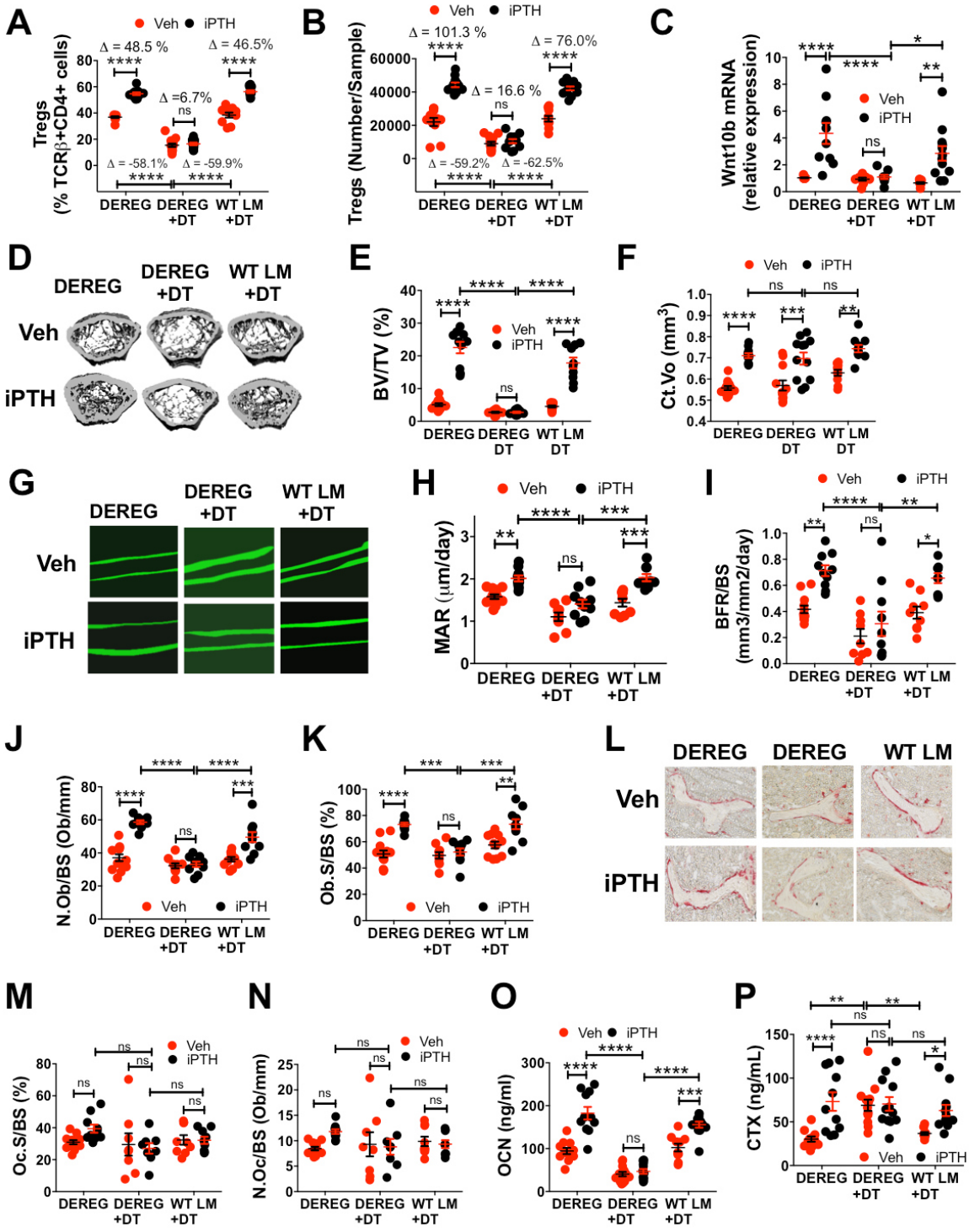

Figure 4. Depletion of Tregs by treatment of DEREG mice with diphtheria toxin (DT) prevents the bone anabolic activity of iPTH. **A,B**. Relative and absolute frequency of BM Tregs. **C.** Wnt10b mRNA levels in BM CD8+ T cells. **D.** Images of representative 3-dimensional μCT reconstructions of examined femurs from each group. **E**. Femoral trabecular bone volume (BV/TV) as measured by μCT scanning. **F.** Femoral cortical bone volume (Ct.Vo) by μCT scanning. **G**. Images are representative sections displaying the calcein double-fluorescence labeling. Original magnification x 20. **H**. Mineral apposition rate (MAR). **I**. Bone formation rate (BFR). **J** The number of osteoblasts per mm bone surface (N.Ob/BS). **K**. The percentage of bone surface covered by osteoblasts (Ob.S/BS). **L**. The images show tartrate resistant acid phosphatase (TRAP) stained sections of the distal femur. Original magnification x 40. **M**. The number of osteoclasts per mm bone surface (N.Oc/BS). **N**. The percentage of bone surface covered by osteoclasts (Oc.S/BS). **O.** Serum levels of osteocalcin, a marker of bone formation. **P**. Serum levels of type 1 cross-linked C-telopeptide (CTX), a marker of resorption. n=9-13 mice per group. Data are expressed as Mean ± SEM. All data were normally distributed according to the Shapiro-Wilk normality test and analyzed by two-way analysis-of-variance and post hoc tests applying the Bonferroni correction for multiple comparisons. *=p<0.05, **=p<0.01, ***=p<0.001 and ****= p<0.0001 compared to the indicated group.

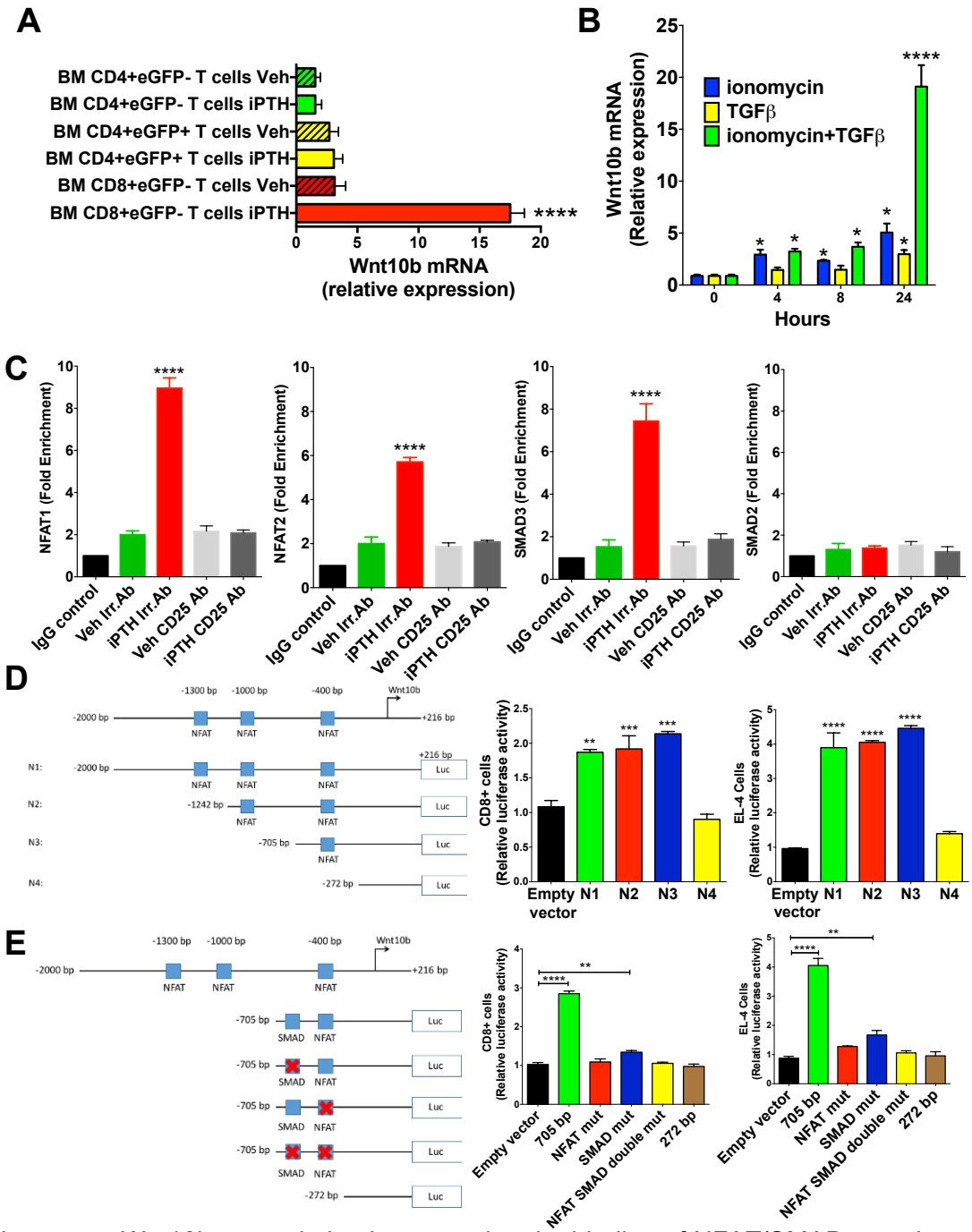

Figure 5. iPTH increases Wnt10b transcription by promoting the binding of NFAT/SMAD complexes to the Wnt10b promoter. A. Expression of Wnt10b mRNA by sorted BM conventional CD4+ cells (TCRβ+CD4+eGFP- cells), Tregs (TCRβ+CD4+ eGFP + cells) and CD8+ T cells from B6.Foxp3.eGFP reporter mice treated with vehicle or iPTH for 4 weeks. **B**. The NFAT activator ionomycin and TGFβ stimulate Wnt10b mRNA expression in splenic CD8+ T cells. **C**. ChIP assays demonstrating that in vivo iPTH treatment increases the binding of NFAT1, NFAT2 and SMAD3, but not of SMAD2, to the Wnt10b promoter in BM CD8+ T cells. Cells from 4-5 mice were pooled to generate 1 sample. **D**. Diagrammatic representation of the Wnt10b promoter and effects of promoter deletion on the activity of Wnt10b-luciferase reporter constructs in primary splenic CD8+ T cells and EL4 T cells. Cells were stimulated with Ionomycin (500 ng/ml) and TGFβ (5 ng/ml) for 24 hours to induce reporter activity. n= 3 samples per group. **E**. Effects of mutation of the SMAD and NFAT binding sites on the Wnt10b promoter on the activity of a luciferase-Wnt10b reporter constructs in primary splenic CD8+ T cells and EL4 cells. Cells were stimulated with Ionomycin (500 ng/ml) and TGFβ (5 ng/ml) for 24 hours to induce reporter activity. Data are expressed as Mean ± SEM. Data were analyzed by Kruskal-Wallis and Dunn's multiple comparisons non-parametric tests, as they were not normally distributed as assessed by Shapiro-Wilk normality test. Panel A: n = 5 per group, ****= p<0.0001 compared the corresponding vehicle group; Panel B: n = 3 per group, * = p <0.05, and ****= p<0.0001 compared the corresponding time 0. Panels C-E: n= 3 samples per group, , **= p<0.01, ***= p<0.001 and ****= p<0.0001 compared to Veh Irr.Ab or empty vector.

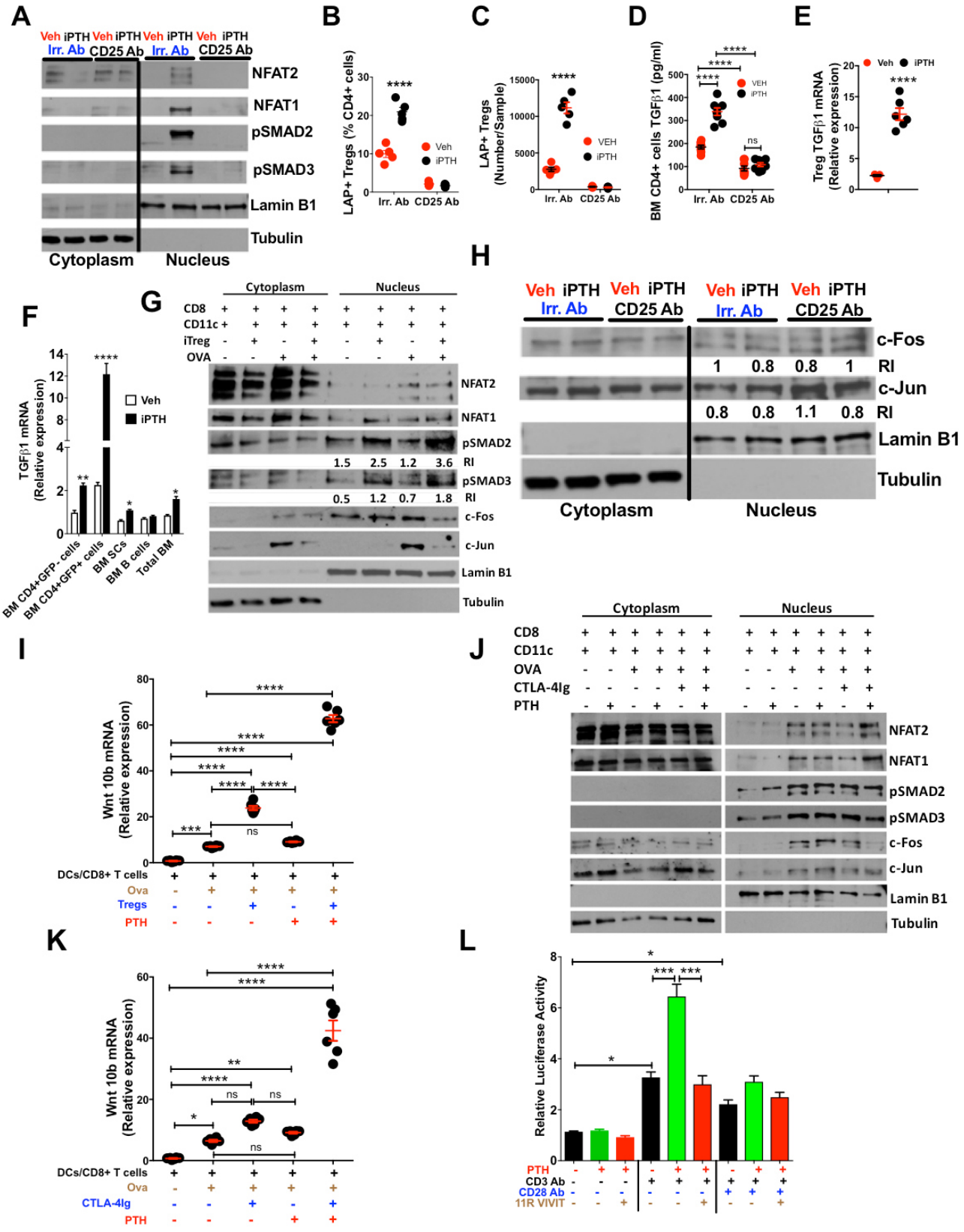
A
Veh iPTH Veh iPTH Veh iPTH Veh iPTH
Irr. Ab CD25 Ab Irr. Ab CD25 Ab
NFAT2
NFAT1
pSMAD2
pSMAD3
Lamin B1
Tubulin
Cytoplasm
Nucleus
B
LAP+ Tregs (% CD4+ cells)
Veh
iPTH
Irr. Ab
CD25 Ab
C
LAP+ Tregs (Number/Sample)
VEH
iPTH
D
BM CD4+ cells TGFβ1 (pg/ml)
ns
E
Treg TGFβ1 mRNA (Relative expression)
F
TGFβ1 mRNA (Relative expression)
BM CD4+GFP- cells
BM CD4+GFP+ cells
BM SCs
BM B cells
Total BM
G
Cytoplasm
Nucleus
CD8
CD11c
iTreg
OVA
NFAT2
NFAT1
pSMAD2
RI
pSMAD3
c-Fos
c-Jun
Lamin B1
Tubulin
H
Veh iPTH Veh iPTH Veh iPTH Veh iPTH
Irr. Ab CD25 Ab Irr. Ab CD25 Ab
c-Fos
RI
c-Jun
Lamin B1
Tubulin
Cytoplasm
Nucleus
I
Wnt 10b mRNA (Relative expression)
DCs/CD8+ T cells
Ova
Tregs
PTH
J
CD8
CD11c
OVA
CTLA-4Ig
PTH
NFAT2
NFAT1
pSMAD2
pSMAD3
c-Fos
c-Jun
Lamin B1
Tubulin
K
Wnt 10b mRNA (Relative expression)
DCs/CD8+ T cells
Ova
CTLA-4Ig
PTH
L
Relative Luciferase Activity
PTH
CD3 Ab
CD28 Ab
11R VIVIT

Figure 6. Effects of PTH and Tregs on NFAT1/2 and SMAD2/3 activation in CD8+ T cells. **A.** Western blotting analysis of NFAT1, NFAT2, pSMAD2, and pSMAD3 in BM CD8+ T cells. The figure shows one representative experiment of 3 experiments. **B,C.** Relative and absolute frequency of BM LAP+ Tregs. **D.** TGFβ1 protein levels in purified BM CD4+ T cells culture media. **E.** mRNA levels of TGFβ1 in BM Tregs. **F**. TGFβ1 mRNA expression by purified BM cells populations. **G**. Western blotting analysis of NFAT1, NFAT2, pSMAD2, pSMAD3, c-Jun and c-Fos in purified splenic CD8+ T cells. CD8+ T cells were unstimulated, activated with OVA peptide pulsed DCs with and without induced Tregs for 2h. The figure shows one representative experiment of 3 experiments. **H**. Western blotting analysis of c-Fos and c-Jun in BM CD8+ T cells. The figure shows one representative experiment of 3 experiments. R.I.= Relative Intensity. **I**. Coculture with induced Tregs increases the baseline and the PTH-induced expression of Wnt10b by CD8+ T cells in an APC assay. **J**. Western blotting analysis of NFAT1, NFAT2, pSMAD2, pSMAD3, c-Jun and c-Fos in purified splenic CD8+ T cells stimulated with PTH (100 nM for 30 min). CD8+ T cells were unstimulated, activated with OVA peptide pulsed DCs with and without CD28 signaling blocking by CTLA-4-Ig treatment. The figure shows one representative experiment of 3 experiments. In panels A,F,G,I, Laminin B1 was used as nuclear loading control. Tubulin was used as cytoplasmic loading control. **K**. Blockade of CD28 signaling by CTLA-4-Ig increases the baseline and the PTH-induced expression of Wnt10b by CD8+ T cells in an APC assay. **L**. Activation of TCR signaling in the absence of CD28 signaling stimulates Wnt10b gene expression in primary splenic CD8+ T cells. The NFAT inhibitor 11R VIVIT blocks Wnt10b gene expression in the absence of CD28 stimulation. Panels B-F and I,K: n = 5-8 mice per group. Data are expressed as mean $\pm$ SEM. Panels B-F and I,K: Data were analyzed by unpaired t-tests or two-way analysis-of-variance and post hoc tests applying the Bonferroni correction for multiple comparisons. Panel L: Data were analyzed by Kruskal-Wallis non-parametric test as they were not normally distributed as assessed by Shapiro-Wilk normality test. * = $p < 0.05$, **= $p < 0.01$, ***= $p < 0.001$ and ****= $p < 0.0001$ compared to vehicle or the indicated group.

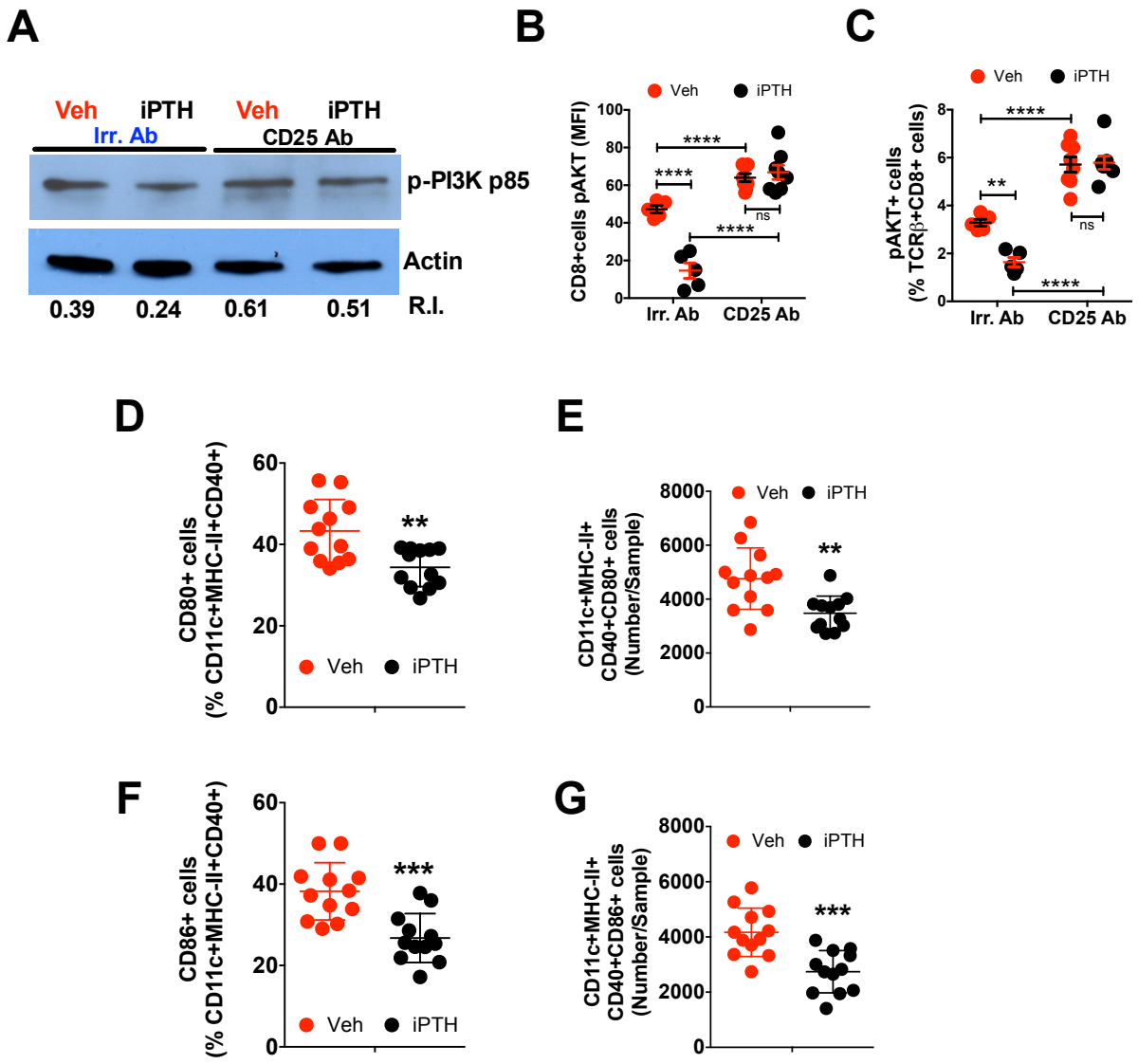

Figure 7. Effects of iPTH treatment on CD28 signaling in BM T cells and the expression of CD80 and CD86 on BM mature dendritic cells (DCs). **A**. Western blotting analysis of Phospho-PI3K p85 in BM CD8+ T cells. The figure shows one representative experiment of 5 total experiments. R.I.= Relative Intensity. **B**. % of pAKT+ BM CD8+ T cells. **C**. pAKT levels in BM C8+ T cells. **D**. Relative frequency of BM CD80+ mature DCs. **E**. Absolute frequency of BM CD80+ mature DCs. **F**. Relative frequency of BM CD86+ mature DCs. **G**. Absolute frequency of BM CD86+ mature DCs. Panels B,C: n = 5-8 mice per group. Panels D-G: n = 12 mice per group. Data are expressed as mean + SEM. Data were analyzed by unpaired t-tests or two-way analysis-of-variance and post hoc tests applying the Bonferroni correction for multiple comparisons. **= p<0.01, ***= p<0.001 and ****= p<0.0001 compared to vehicle or the indicated group.

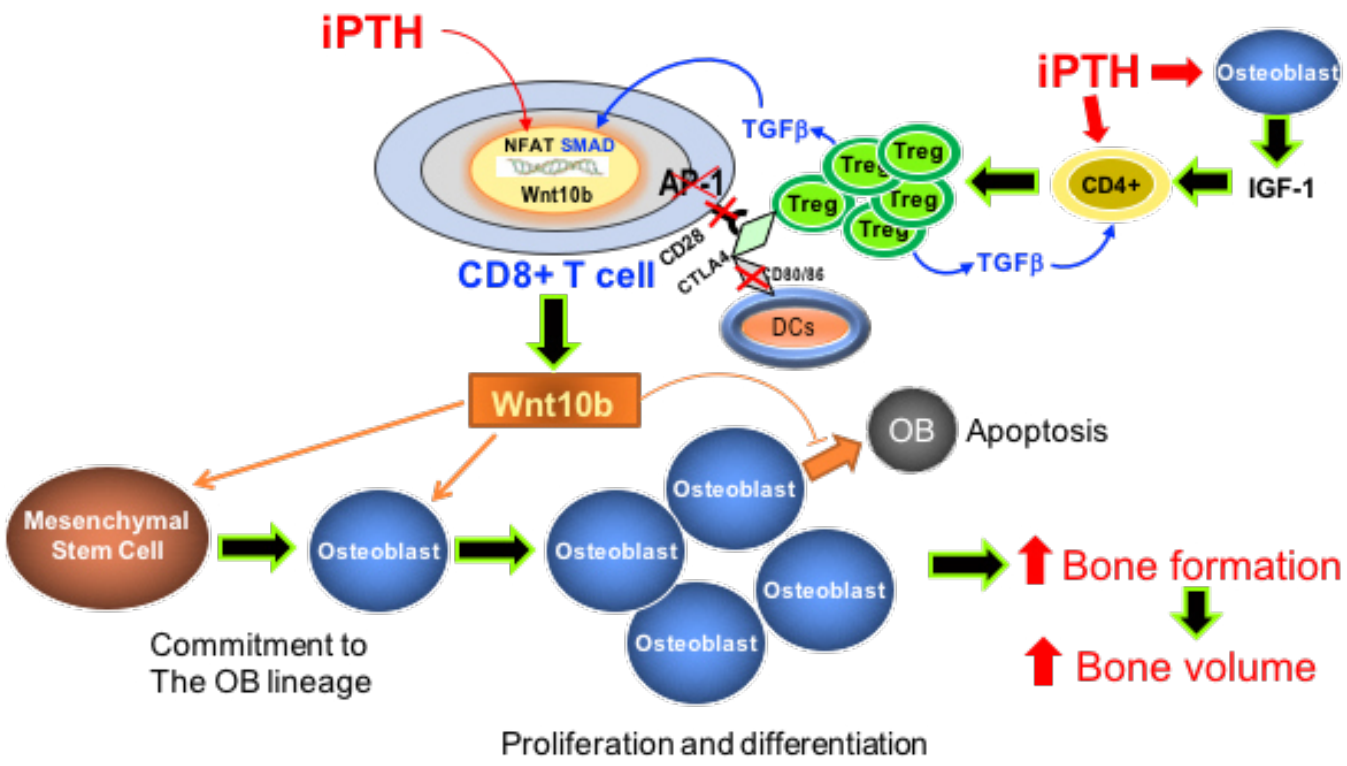

Figure 8. Diagrammatic representation of the mechanism by which iPTH treatment stimulates bone formation and increases bone mass. iPTH increases the differentiation of naïve CD4+ T cells into Tregs and expands the pool of BM Tregs by up-regulating the production of IGF-1 and TGFβ in BM microenvironment and by increasing the sensitivity of conventional CD4+ T cells to TGFβ. mature Tregs do not express PPR and are not directly targeted by iPTH. Membrane-bound TGFβ produced by Tregs activates SMAD signaling in CD8+ T cells while iPTH activates NFAT signaling in CD8+ T cells. Moreover, Tregs downregulate CD28 signaling in CD8+ T cells, lowering the activation of AP-1, thus preventing the association of NFAT and AP-1. In such conditions of low AP-1 levels, NFAT bind together with SMAD to the Wnt10 promoter activating Wnt10b transcription. Direct stimulation of CD8+ T cells by iPTH further upregulate Wnt10b gene expression. Wnt10b is known to activate Wnt signaling in mesenchymal stem cells and their osteogenic progeny, leading to increased osteoblast proliferation and differentiation and lower osteoblast apoptosis. This increase in osteoblastogenesis and osteoblast life span increases bone formation and bone trabecular bone volume.